Analyzing the chemical composition, morphology and size of ice-nucleating particles by coupling a scanning electron microscope to an offline diffusion chamber

Lisa Schneider[1], Jann Schrod[2], Daniel Weber[2,a], Heinz Bingemer[2], Konrad Kandler[1], Joachim Curtius[2], Martin Ebert[1]

[1]Institute of Applied Geoscience, Technical University of Darmstadt, Darmstadt, 64287, Germany
[2]Institute for Atmospheric and Environmental Sciences, Goethe University Frankfurt, Frankfurt am Main, 60438, Germany
[a]now at: Federal Waterways Engineering and Research Institute, Karlsruhe, 76187, Germany

Correspondence to: Martin Ebert (mebert@geo.tu-darmstadt.de)

Abstract. To understand and predict the formation of clouds and precipitation and their influence on our climate, it is crucial to know the characteristics and abundance of ice-nucleating particles (INPs) in the atmosphere. As the ice-nucleating efficiency is a result of individual particle properties, a detailed knowledge on these properties is essential. Here, an offline method for the comprehensive single particle analysis of ambient INPs that benefits from the combination of two instruments already used for ice nucleation measurements is presented, focusing on the methodological description of the coupling, whereby strengths and weaknesses of the method are discussed.

First, the aerosol is sampled on silicon wafers. INPs are then activated at different temperature and humidity conditions in the deposition nucleation and condensation freezing mode using a static diffusion chamber. The positions of grown ice crystals are defined by a coordinate system, which allows for recovery and detailed analysis of the individual INPs by a scanning electron microscope. Based on their physico-chemical properties (chemistry and morphology) the INPs can be classified into categories. In combination with the size information, a size-resolved distribution of the INP classes can be determined. Such results are useful for evaluating INP type-specific parametrizations, e.g., for use in atmospheric modeling, and in closure studies.

A case study from the high-altitude research station Jungfraujoch, Switzerland shows that the targeted INP analysis as obtained by this method is able to identify the main INP classes in reliable proportions. Most of the deposition nucleation / condensation freezing mode INPs activated at -30 °C, indicated a geogenic mineral origin (mainly aluminosilicates / Al-rich particles, but also carbonates and silica). Other major contributors were carbonaceous particles, consisting of both smaller soot particles and larger biological particles, and mixed particles (mostly Al/C mixed particles). The INPs had projected area diameters ranging from 300 nm to 35 µm, with a distinct maximum at 1 - 2 µm. Mineral particles were present throughout the entire size range, while mixed particles were identified in higher abundances at sizes of 3 µm and above. Minor contributions were seen from sulfates and metal oxides, the latter with an increased proportion in the size range below 500 nm. During a Saharan dust event, a significant increase of mineral particles in the INP composition was detected.

1 Introduction

Ice-nucleating particles (INPs) have a significant impact on climate and weather. They influence cloud formation and thus have an effect on cloud structure, extent and lifetime, as well as on radiation and precipitation properties (Kanji et al., 2017, and references therein).

Ice formation in the atmosphere can be initiated via several mechanisms depending on ambient conditions. At temperatures below approximately -38 °C, supercooled solution droplets may freeze spontaneously without a crystallization nucleus (homogeneous freezing). To start ice formation at warmer temperatures (T > -38 °C), the energy barrier for nucleation has to be reduced. This can be accomplished by the presence of an INP. Conventionally, four mechanisms are distinguished for heterogeneous freezing processes: (1) deposition nucleation, (2) condensation freezing, (3) contact freezing and (4) immersion freezing. Detailed information on ice nucleation terminology can be found in Vali et al. (2015) and Kanji et al. (2017).

Only a small fraction of the total aerosol can act as INPs and their concentrations can show variations of several orders of magnitude in space and time (DeMott et al., 2010; Kanji et al., 2017). In addition to the prevailing environmental conditions i.e., temperature and humidity, the potential for an INP to become activated is dependent upon individual particle properties (surface imperfections (Kiselev et al., 2016), chemical composition and specific chemical properties, crystal structure, coating (Kanji et al., 2008), etc.) as well as its atmospheric processing including potential agglomeration or pre-activation (Marcolli, 2017). The promoting sites on the surface of an INP are termed active sites. As particle size increases, the number of active sites also tends to increase. So typically, the larger an atmospheric particle is, the more likely it is to act as an INP (Archuleta et al., 2005; Welti et al., 2009).

Ice-forming activity has been verified for many atmospheric particle classes. Mineral dust, which is emitted from arid and semi-arid regions and is globally distributed in the atmosphere (Perry et al., 1997; Ansmann et al., 2003; Schepanski et al., 2018), is a good INP at temperatures below -15 °C (Hoose & Möhler, 2012). The composition of mineral dust is highly variable depending on the source region (Scheuvens & Kandler, 2014). Furthermore, soil dust (mineral dust which is often mixed internally with organic components) from agricultural regions is regarded to be a source of INPs (O'Sullivan et al., 2014). Metal oxides can be components of mineral dust from natural sources and are also emitted by anthropogenic sources. Their efficiency to activate as INPs depends on the type of metallic cation as well as on the oxidation state (Archuleta et al., 2005; Yakobi-Hancock et al., 2013). At temperatures warmer than -15 °C, mainly biological INPs are ice active (Després et al., 2012, and references therein). These include primary particles such as bacteria, fungal spore, pollen and plant debris, as well as some biological macromolecules (Pummer et al., 2012). Particles from biomass burning and fossil fuel combustion are considered as another particle class relevant for ice formation. This includes soot (mostly a mixture of black carbon with organic carbon) as a product of incomplete combustion as well as fly ash from the non-combustible components. However, the contribution of soot to atmospheric ice formation is still subject of discussion, e.g., Cozic et al. (2008) and Kupiszewski

et al. (2016) found opposing results at the same location. Besides the continental sources, the oceans also serve as a source for atmospheric INPs. In addition to sea salt, sea spray aerosol also contains increased amounts of marine organic material from the sea surface microlayer, which is considered to have significant ice-nucleating properties (Wilson et al., 2015). A detailed overview of all atmospherically relevant INPs is given by Kanji et al. (2017) and Burrows et al. (2022).

Although there is a variety of methods to determine the INP concentration in the laboratory (Hoose & Möhler, 2012; Hiranuma et al., 2015; DeMott et al., 2018; Hiranuma et al., 2019) and in the field (Wex et al., 2019; Schrod et al., 2020b; Brasseur et al., 2022; Lacher et al., 2024), only a few of them are simultaneously able to report on the chemical characteristics of individual ice-nucleating particles.

Most analytical methods for the chemical characterization of ambient ice nuclei are based on the principle of first separating the ice nuclei or ice particles from the total atmospheric aerosol using different approaches. Ice crystals can be separated directly from clouds by using specialized inlets (Schwarzenböck et al., 2000; Mertes et al., 2007; Schenk et al., 2014; Kupiszewski et al., 2015). In this case, the particles are heated after separation so that the water evaporates and ice residuals (IR) remain. In another approach, the particles are activated under defined conditions in an online reaction chamber (e.g., Rogers, 1988) after the collection of the total aerosol. To analyze the activated particles, it is necessary to separate the ice crystals from droplets and evaporate the ice by one of the specialized inlet systems or a droplet evaporation zone.

In a second step, the separated INPs/IRs are then either analyzed in the air stream or separated and transferred to an offline analysis. To our knowledge, the only online experiment that has been used to determine all particle groups relevant to ice nucleation simultaneously is single particle mass spectrometry (SPMS) (Thomson et al., 2000; Kamphus et al., 2010; Brands et al., 2011). In general, online methods allow a real-time analysis with the potential of high time resolution but may have problems at low INP concentrations. However, several studies have reliably demonstrated the coupling between a separation technique and SPMS in a field setting (Cozic et al., 2008; Pratt et al., 2009; Cziczo et al., 2009; Kamphus et al., 2010; Cziczo et al., 2013; Schmidt et al. 2017; Lacher et al. 2021). Electron microscopy (EM), as an offline method, offers an alternative approach to study the chemical composition of INPs/IRs. For single particle analysis by EM, INPs or IRs are collected on substrates after evaporating the ice phase. Single particle analysis can be performed automated for large data sets or manually with operator control (Eriksen Hammer et al., 2019). Even though the method cannot provide high temporal resolution measurements due to longer sampling times, it can provide detailed information on morphology in addition to chemistry and size of individual INPs and IRs (Mertes et al., 2007; Prenni et al., 2009; Cziczo et al., 2009; Ebert et al., 2011; Cziczo et al., 2013; Worringen et al. 2015; Eriksen Hammer et al., 2018).

These methods typically analyze large numbers of INPs/IRs. However, the major challenge of all these methods is that due to the extremely low number of INPs within a sampled air volume compared to the much higher number of non-INP particles (ratio ~ $1/10^4$ – $1/10^6$), the separation must be carried out with a very high accuracy. Even with an accuracy of 99.9 % for INP separation, this would mean that for every correctly separated INP 1000 non-INP particles would be separated incorrectly, when an INP to total aerosol ratio of $1/10^6$ is assumed. In this way, no conclusions about the chemistry

of the INP would be possible at all, since there is no way to distinguish particles that have been falsely separated as INP from real INP afterwards. There is also the risk that additional artifacts can be introduced into the INP fraction during the multi-step process. This problem is partially illustrated in the comparison of the chemical analysis of the INP/IR fraction by three different methods in Worringen et al. (2015).

This paper describes an offline method for measuring atmospheric INP concentration in combination with a subsequent characterization of the activated INPs. The recently established method couples the ice nucleation counter FRankfurt Ice nucleation Deposition freezinG Experiment (FRIDGE) to a scanning electron microscope (SEM). With this method, individual particles can be specifically analyzed, of which it is known that the ice formation has taken place on the substrate exactly at their position. The FRIDGE-SEM-coupling technique has been used for several campaigns in recent years, providing valuable results (Schrod et al., 2017; Schrod et al., 2020b; Weber, 2019; He et al., 2023). Details of the FRIDGE method were described by Schrod et al. (2016).

The present publication expands significantly on these studies by detailing the technical procedure to gain reliable information on physico-chemical properties of INPs by SEM, which were previously activated in FRIDGE. The first part of the paper presents a detailed description of the FRIDGE-SEM coupling - highlighting the strengths and discussing the weaknesses - followed by the results of a case study from the high-altitude research station Jungfraujoch (JFJ), Switzerland in 2017.

2 Methodology: Coupling a scanning electron microscope to an ice nucleus counter

The here presented offline coupling procedure (Fig. 1) combines the advantage of two devices which are already used for several years in the field of INP/IR research. Particles can be collected from ambient aerosol onto substrates by electrostatic precipitation (Fig. 1A). The sampled aerosol is then analyzed with respect to its ice nucleation ability at various combinations of activation temperature and supersaturation with respect to ice, yielding the INP concentration (Fig. 1B). The activated INPs can subsequently be characterized by SEM to gain information on their chemistry, morphology and size (Fig. 1C). Based on the definition by Cziczo et al. (2017) we refer to the identified particles as INP, as they were activated under defined conditions after the collection of the total aerosol and not sampled as ice crystals. Therefore, we are able to investigate truly activated particles in contrast to methods analyzing IRs, which face challenges in order to distinguish between IRs and scavenged particles. However, some of the INPs analyzed with SEM may have undergone changes due to the measurement procedure in FRIDGE, but we assume that these changes are of minor importance for the main INP classes that we can analyze with this method (see Sect. 2.6).

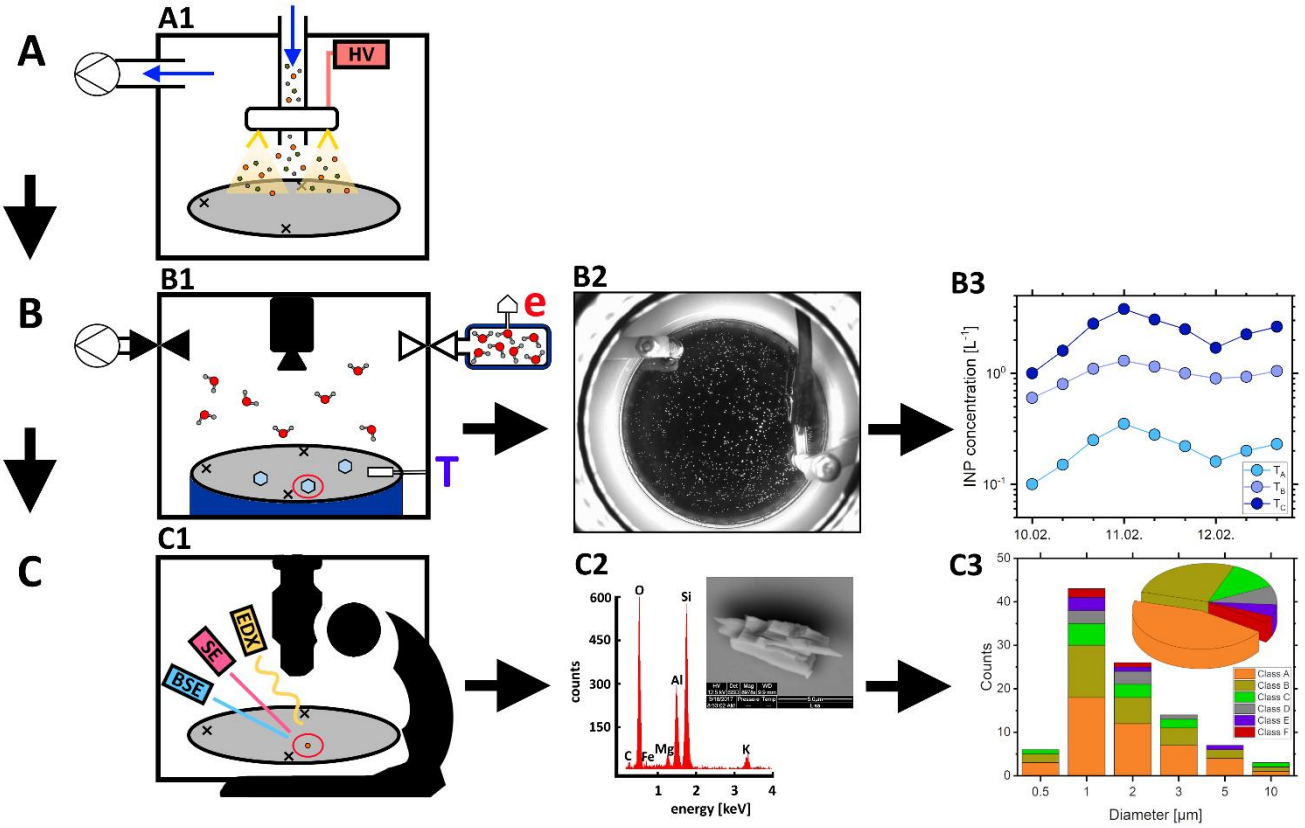

Figure 1: Schematic for the coupled INP analysis. (A) Electrostatic Aerosol Collector (EAC): The aerosol (colored particles) is pumped through the sampling unit in the direction of the blue arrows. By applying a high voltage (HV), gold filaments (yellow) arranged in a ring generate an electrostatic field (light yellow triangles). The charged particles are deposited on the silicon substrate (gray). (B) FRIDGE: Diffusion chamber setup (B1) with silicon substrate (gray) placed on the cold stage (dark blue) equipped with a temperature sensor (T). The water vapor pressure (e) in the water vapor source (top right) is measured with a pressure sensor. A vacuum pump (top left) is used to evacuate the reaction chamber before the measurement starts. Starting a measurement, the valve to the water vapor source is opened, the diffusion chamber gets flooded with water vapor (red/grey molecules) and ice crystals (light blue) start to grow on the substrate. A camera (top center) monitors the ice growth and records images (B2). This can be used to calculate an INP number concentration for different temperature and humidity settings (B3). (C) SEM: Silicon substrate (grey) with the three engraved crosses defining the coordinate system, placed in the scanning electron microscope (black schematic) equipped with several detectors (solid state detector (blue), Everhart-Thornley detector (red) and energy dispersive x-ray detector (yellow)) (C1). Each individual INP which induced ice crystal growth in FRIDGE (particle circled in red) is chemically and morphologically analyzed. The result is a secondary- and backscattered-electron particle image and an elemental spectrum (C2). As a final result, all the individual particle information is combined in a bulk chemical composition and a chemically-resolved size distribution (C3).

2.1 Sample substrates

A silicon disk with a diameter of 45 mm serves as the sample substrate, on which the aerosol particles are deposited by electrostatic precipitation (see Sect. 2.2). The semi-conductive substrate is made from commercially available silicon wafers, which are widely used as basis for microchips in electronic devices. The pure crystalline silicon surface is highly inefficient for ice-nucleation, which prevents random icing on the wafer, that would induce an artificial background signal and would lead to incorrect INP concentrations. The extremely smooth wafer surface allows for an unambiguous separation of particles from the background in the electron microscope. Each wafer is marked with three laser-engraved crosses near the edge, which span a 90° angle. These markers define a coordinate system, which allows for the precise localization of the ice-nucleation spots (Sect. 2.4).

After analysis, the wafer substrates are cleaned in a simple two-step process and can be reused subsequently. For this, wafers are pre-cleaned with ethanol and laboratory wipes (Kimtech Science, 7557, Kimberly-Clark) to eliminate oil residues from previous measurements and other coarse contamination. Then, in order to remove fine particles from the surface, the substrates are treated with a beam of dry ice crystals (Sno-Gun II, Va-Trans System, Inc.). The cleaning procedure is performed inside a particle free work space (SPECTEC, laminar flow box FBS). To verify the cleaning process, randomly selected cleaned wafers are analyzed in the ice nucleation chamber. However, even after thorough cleaning a small amount of ice formation can regularly be observed at temperatures at or below -30°C, constituting the background concentration and defining the limit of detection, which is in the order of 0.1 L^{-1} of atmospheric air for a collection volume of 100 L.

2.2 Electrostatic Aerosol Collector

Aerosol is precipitated onto the substrates using an Electrostatic Aerosol Collector (EAC) (Klein et al. 2010). Several EACs have been deployed for the use in the laboratory (DeMott et al., 2018), in field campaigns (DeMott et al., 2024), for measurements with unmanned aerial vehicles (Schrod et al., 2017), and for long-term observations at research stations (Schrod et al., 2020b). The most recent version, which was also used in the case study (Sect. 3), PEAC7, is a programmable EAC (Schrod et al., 2016) designed for semi-automated operation for one week of daily sampling.

Inside the collection unit, sample air passes through the corona discharge unit, which charges the particles negatively when a high voltage of about 12kV is applied. Charged aerosol particles follow the electric field to the grounded plate and are deposited on the silicon wafer substrate (Fig. 1A). This sampling process leads to a rather homogeneous particle distribution on the wafer, which is of great importance both for the measurements in the ice nucleation chamber and for the later individual particle analysis by EM. However, not all particles are deposited on the wafer during electrostatic precipitation, some are deposited elsewhere in the system. Characterization experiments determined a size-independent collection efficiency of 60 % in the 0.5-3 µm size range (Schrod et al., 2016).

2.3 FRIDGE

The FRankfurt Ice nucleation Deposition freezinG Experiment (FRIDGE) is an offline isostatic vacuum diffusion chamber in which the activation of atmospheric INPs and the associated growth of ice crystals can be observed and documented under laboratory conditions (Bundke et al., 2008; Klein et al. 2010). The diffusion chamber addresses the deposition nucleation and condensation freezing modes (re-evaluated by Schrod et al., 2016), but the instrument can also be used in a different setup as a droplet freezing device to address the immersion freezing mode (Boose et al. 2016; Schrod et al., 2020a). As the immersion mode setup is not subject of our study, the following section describes the measurement procedure for the deposition nucleation and condensation freezing modes (schematic shown in Fig. 1B), with a particular emphasis on the desired coupling.

For coupling the INP activation experiment to the single particle analysis, it is important to keep the three laser-engraved crosses on the wafer surface visible during the FRIDGE measurement. The temperature sensor (PT1000) is therefore attached opposite to the middle cross, (see Fig.1 - B1). A small amount of silicon oil is applied on the bottom of the wafer as well as on the temperature sensor to ensure good thermal contact and a homogeneous temperature distribution. When the chamber is evacuated and the selected activation conditions are stable, the water vapor diffuses into the cold chamber, activating the INPs on the wafer surface. The growth of ice crystals is observed as a function of time (time step of 10 s) by a CCD camera (2/3" CCD ≥ 5 megapixels, 1 pixel ≈ 400 μm^2) placed above the reaction chamber. Ice crystals are identified by an image analysis software (LabView) comparing the brightness of new objects to a previously recorded reference image. Details can be found in Schrod et al. (2016). For the coupling procedure it is beneficial to stop the growth of ice before individual ice crystals grow to large sizes or coalescence, because the determination of the ice crystal center (Sect. 2.4), which is assumed to be the position of the INP, is more precise with small crystals. Additionally, this also reduces the spatial extent of potential particle drift during the ice crystal growth. By directly evaporating the ice crystals at the end of a measurement cycle with the objective of avoiding the liquid phase, the risk of possible particle drifts is also reduced.

As a routine, the wafers are measured in 12 cycles combining 3 temperatures (T = -20 °C, -25 °C, -30 °C) and four relative humidity (RH) settings each (RH = 95 %, 97 %, 99 %, 101 %). An efficient evacuation between measurement cycles is necessary to ensure the complete water evaporation from the particles to avoid pre-activation effects from residual water/ice in microscopic cavities on the particles surface (Jing et al., 2022). Based on the ice crystal numbers, the collection volume and the PEAC7 sampling efficiency, the INP concentration at different temperature and humidity settings is calculated.

For the subsequent EM with energy dispersive x-ray spectroscopy, it is important to completely remove the oil from the edge and underside of the wafer after the FRIDGE measurements, as otherwise the chemical analysis of the INPs can be influenced by the evaporating oil. Because of this oil-removing step, the edge and the area of the temperature sensor are excluded from further analysis.

2.4 Identification of ice crystal positions

In order to be able to match the ice crystals formed in FRIDGE to the corresponding ice-nucleating particles with SEM, the origin of each ice crystal must be located by a coordinate system based on the FRIDGE images. Therefore, a homogeneous distribution of ice crystals on the substrate with an adequate range of crystal density is favorable. The steps described below apply to such favored conditions.

The ice crystal positions are identified by image analysis using the internal particle analyzer of the free image processing software ImageJ (Schneider et al., 2012), with a minimum size of 30 pixels proven to be useful. The reference points of the coordinate system have to be defined manually by tagging the centers of the three crosses in a reference image as their non-uniformity prevents an automated approach. The software identifies the image with the highest number of ice crystals for each measurement cycle and tags the ice crystal positions in the images as the center of the detected bright area. These positions are translated into relative coordinates defined by the calibration marks. It can be assumed that this coordinate represents the position of the corresponding INP, since an approximately radially symmetric ice crystal growth can be observed in the range of the selected activation conditions in FRDGE. Nevertheless, a potentially imperfect radial symmetry of the ice crystal growth, coupled with the restricted resolution of the FRIDGE images (20 x 20 µm), may result in an uncertainty in the calculation of the ice crystal origin. As the size of an ice crystal increases, the probability and extent of such a non-symmetrical growth also increases. The quantification of this uncertainty proved to be difficult, as it depends on the symmetry deviation present. To reduce this uncertainty based on an imperfect radial symmetry, the ice crystal position calculation should be performed on the basis of FRIDGE images, that show the ice crystals in a state close to activation.

Figure 2 shows a comparison between the number of ice crystals counted by FRIDGE and the number of ice crystal positions calculated for the SEM analysis. Usually, almost all ice crystal positions calculated by the counting algorithm can be related to real grown ice crystals, defined as clearly visible bright objects, which continue to grow in the ice supersaturated regime as the measuring time progresses. The few deviations are caused by various reasons. Higher numbers of ice crystal positions calculated for SEM can be caused by misclassifying areas with condensation, which may occur while working close to RH = 100 %. A lower number of ice crystal positions calculated for SEM is often caused by ice crystals that have grown together due to prolonged measurement in FRIDGE or by the presence of ice crystals in close proximity to one another, resulting in only one position for two or more crystals (see also Fig. S1). These Positions are excluded from further analysis.

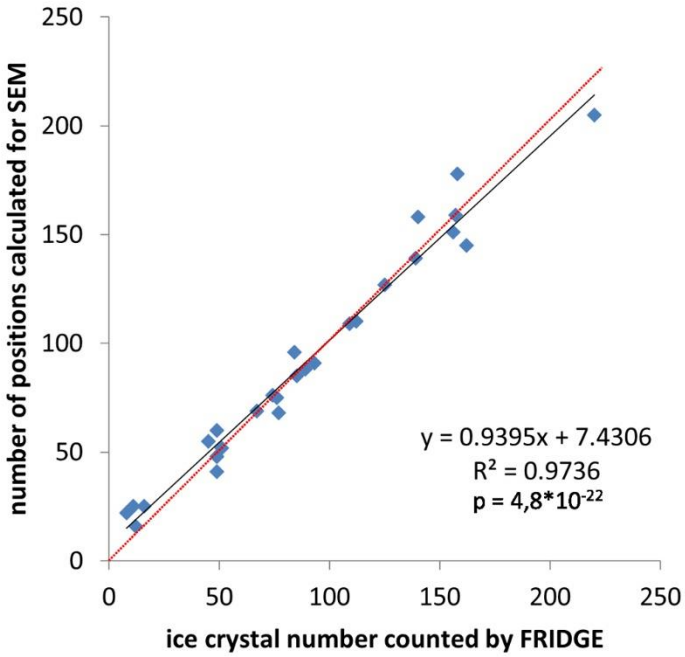

Figure 2: Comparison of ice crystal numbers detected by FRIDGE with the number of positions calculated for SEM analysis . The 1:1-line is shown in red.

2.5 Scanning Electron Microscopy

A Quanta 200 FEG Environmental Scanning Electron Microscope (ESEM) by FEI (Field Electron and Ion Company; Eindhoven, Netherlands) coupled to an energy dispersive X-ray detector (EDX) (EDAX, AMETEK, Tilburg, Netherlands) was used for analysis. The instrument is also equipped with an Everhardt-Thornley detector (ETD) which maps the topology of a particle by secondary electrons (SE) and a solid-state detector (SSD), providing the distribution of elements on the particle by backscattered electrons (BSE) giving information on homogeneous or heterogeneous distribution of elements and on inclusions. The EDX provides an elemental composition of an individual particle, which can be used to attribute the analyzed particles to different classes of composition and origin. As all analyses were carried out in high vacuum (10^{-6} mbar), the instrument is referred to as SEM in the following. The acceleration voltage was 12.5 kV or 15 kV, the working distance was 10 mm as standard.

2.5.1 Coordinate calibration

As the internal SEM coordinate system is centered around the origin in the middle of the stage aligning the axes to the directions of mechanical movements, it is necessary to perform a coordinate transformation to link the SEM coordinates to the coordinates defined by the crosses in the previous step. Based on a calibration image, which indicates the marked center points from the previous ice crystal identification step (Sect. 2.4), these calibration points have to be transferred to the SEM.

It is highly important to locate these points with high precision, since the position of each ice crystal in the subsequent analysis is based on this conversion. Manual calibration provides the highest precision, as the different physical imaging processes between the two instruments and the high magnification of the electron microscope in contrast to the limited resolution of the FRIDGE calibration picture, impair any precise automated calibration. Due to the limited resolution of the FRIDGE images of about 20 x 20 µm, the calibration has of course an uncertainty in the same order of magnitude.

2.5.2 INP identification

Each ice crystal position, based on a real grown ice crystal, is inspected by SEM to identify the presence of particles. Given the uncertainties associated with the ice crystal identification process (Sect. 2.4) and the coordinate calibration (Sect. 2.5.1), it is crucial to consider not only the exact calculated coordinate but also the surrounding area. This area must take into account the aforementioned uncertainties and, at the same time, limit the probability that several particles will be observed in the scanned area. In this context, a radius of 50 µm has proven to be useful. While the previously discussed uncertainties may suggest a lager radius to be beneficial, in fact, the high substrate loading often proves to be the limiting factor. Since the substrate loading depends strongly on the prevailing total aerosol concentration at the sampling location, the conditions for analysis can be optimized by adjusting the scanning radius for different wafer loadings.

While scanning the calculated ice crystal position for particles, three cases can be distinguished:
(1) If one single particle is found within the specified radius, it is considered to be the corresponding INP. If the BSE-image, in which the contrast depends on chemistry, indicates chemical differences within the particle, multiple EDX spectra of the different areas are recorded (Fig. 3 and Fig. 4). The comprehensive single particle analysis (Sect. 2.6) enables the identification of physico-chemical properties that may be pertinent to ice formation.
(2) If more than one particle is identified within the defined area around the coordinate, it is not possible to make a definite allocation of the INP. These positions have to be excluded from the analysis.
(3) In the absence of a particle within the 50 µm radius, these blank positions are typically disregarded. A blank position may be the consequence of possible particle drift during the processing in FRIDGE (Sect. 2.3), or the result of an erroneous calculation of the ice crystal origin (Sect. 2.4). Nevertheless, in instances where the substrate loading is low, extending the screening radius in the case of a blank position may be beneficial in increasing the number of identified INPs.
Figure 3 illustrates a result from the INP identification step with the SEM, based on the corresponding FRIDGE picture with the grown ice crystals.

The number of INPs that can be unambiguously attributed to an ice crystal origin is significantly influenced by the total wafer loading, which is determined by the sampling parameters (e.g., flow rate, sampling time, deposition efficiency) in combination with the aerosol concentration present. However, even if the aerosol concentration is known, it is difficult to specify a suitable collection volume in advance, as the ratio of potential INPs to the total aerosol also plays a role. This ratio

is variable and usually unknown prior to measurement. As a result, the amount of atmospheric aerosol and the proportion of INPs deposited on a wafer are highly variable. This variability is also seen in the identification rates, which is why it would be misleading to give an average identification rate for the method presented. However, a specific identification rate for the case study conducted at the high-altitude research station Jungfraujoch (Sect. 3) can be given here as a guideline. The average INP identification rate was calculated to be 30% (ranging from 13 % to 50 %). Furthermore, the study identified the presence of multiple particles at 45 % of the locations (ranging from 7 % to 81 %), while the remaining 25 % (ranging from 2 % to 66 %) were found to be blank positions.

Based on the uncertainties and assumptions discussed, many positions and potential INPs are excluded from further analysis, which leads to the limited number of identified INPs per sample. However, these INPs are identified with a high degree of accuracy as we know that ice formation has taken place on the substrate at their position. In most cases, the small number of clearly identified INPs still allows general statements to be made, e.g., about the most frequently occurring characteristics of INPs (e.g., predominantly silicates or predominantly sub-µm particles), but often no general statement about rarely occurring subgroups of INPs are possible (see Sect.3).

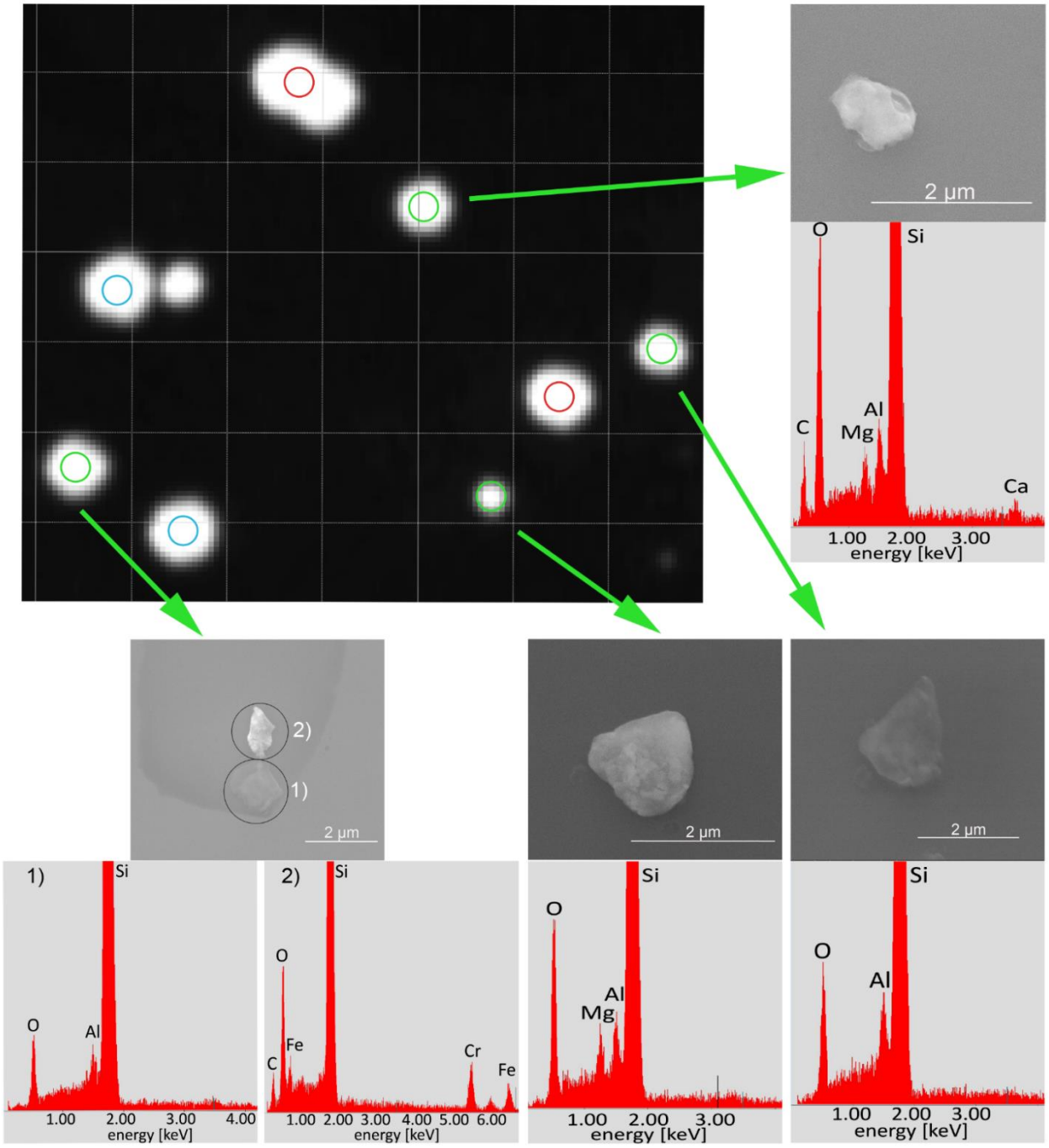

Figure 3: FRIDGE picture (resolution 20 x 20 µm) showing grown ice crystals including one coalesced crystal (top center). The corresponding scan radius of 50 µm from SEM is shown by the colored circles: Blank positions (red), multiple particle positions (blue) and identified INPs (green). However, one ice crystal was not detected by the ice crystal identification software. For the identified INPs, the corresponding pictures and EDX spectra are shown. For one particle (bottom left), the BSE image indicates a different chemical composition, so two spectra were recorded.

2.6 Individual particle analysis

The analysis by SEM and EDX is an efficient method for characterizing INPs in detail, as it provides information on elemental composition and distribution as well as on morphology and surface properties. With this detailed information, it is possible, for example, to determine the mixing state of a particle (see Fig. 3 and Fig. 4). The morphological information can be used for source apportionment (e.g., for biological particles, soot, spherical particles from high temperature processes).

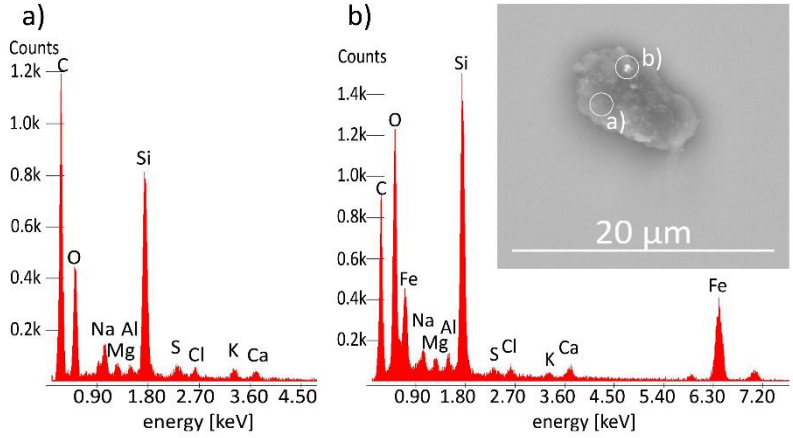

Figure 4: EDX spectra and BSE image of a C-rich INP (a) with Fe-rich areas (b).

The size of the INPs is determined in the last step of the coupling method from the SE/BSE pictures. The INPs have been processed in FRIDGE (multiple activation/evacuation cycles) and they were analyzed in a high vacuum under the electron beam. Therefore, the morphology of the particles may have undergone alterations. This may be especially the case for soluble/volatile components within a sample, which may evaporate during the analysis procedure. It can be assumed that these changes are of minor importance for most of the INPs classes that can be determined using this method.

In the following section we define a classification scheme, which is mainly based on elemental composition (Fig. 5) and in some cases on the morphology of particles (Fig. 7). The subgroups defined in Fig. 5 can be summarized in three main groups (mineral particles, carbonaceous particles and other particles). It should be noted, however, that it is not possible to quantify the silicon content of a particle with this method. Given that we are working on a silicon substrate, a Si background signal in the resulting spectrum is always present. This may limit the chemical characterization of particles with a very small size, as their element signals with respect to the background signal may be insufficient. Instability with respect to the electron beam also leads to limited detection of particle properties.

Based on the research question or the occurrence of specific particle classes at the sampling site, the classification scheme may be adapted.

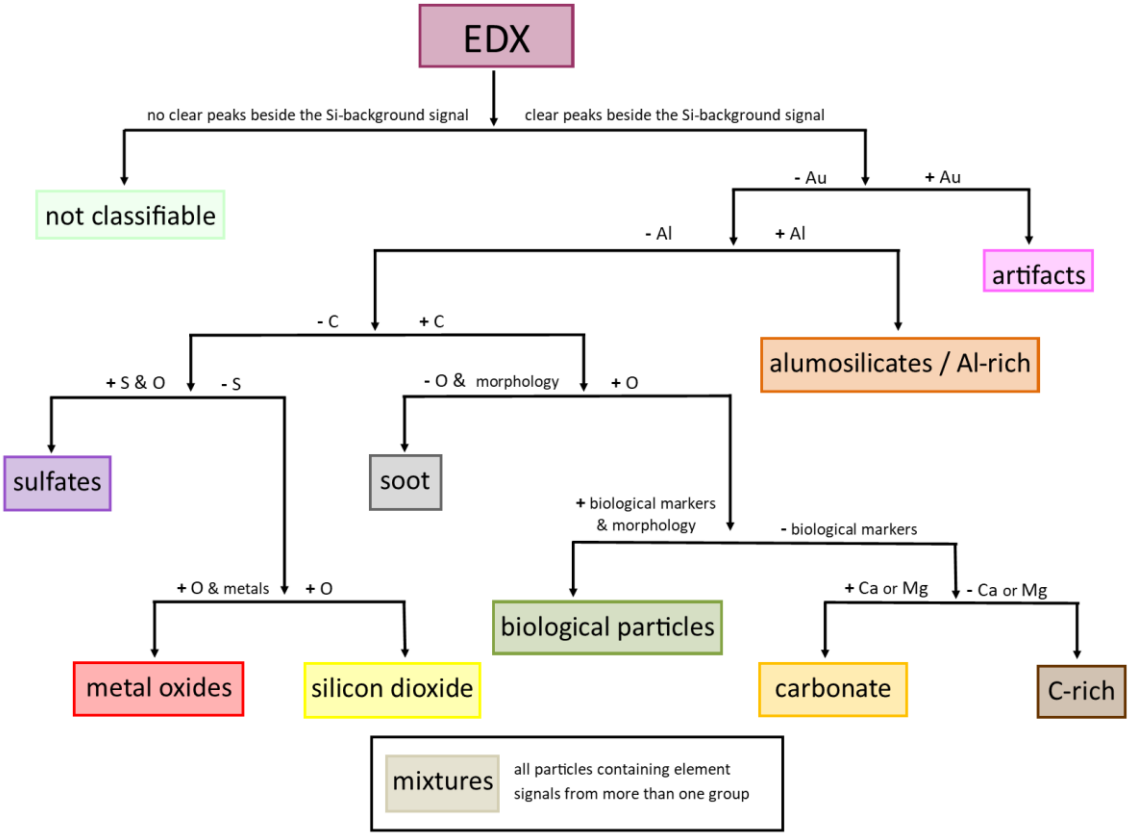

Figure 5: INP classification scheme.

Mineral components

Aluminosilicates / Al-rich particles, carbonates and silicon dioxide are summarized as mineral components. Typically, their irregular structure indicates a geogenic origin.

The *aluminosilicate / Al-rich* group is identified based on the Al signal and represents a combined group, as it is not possible to quantify the silicon content of a particle. The dominating source for aluminosilicates in the atmosphere is mineral dust from arid and semi-arid regions, while Al-dominated particles are usually rare (Okada & Kai, 2004; Kandler et al., 2007). In case of aluminosilicates, the particles may contain several minor elements (e.g., Na, Mg, K, Ca, Fe) in different ratios (Fig. 6), depending on the minerals from which they originate. Their internal element distribution may be not homogeneous. This method can therefore be used to estimate the abundance of individual mineral components in the INP fraction, potentially identifying an enrichment of highly effective ice nucleating particles (e.g., K-feldspar).

Carbonates can contain, in addition to carbon and oxygen, different counterions (e.g., calcium and/or magnesium), based on the mineralogical origin (e.g., calcite, dolomite).

Silicon dioxide is identified by the presence of only oxygen alongside - the not quantifiable - silicon. A distinction between different particle sources can be made on the basis of their morphology. While most geogenic quartz particles show irregular shapes with typical sharp edges (Whalley and Krinsley, 1974), anthropogenic SiO_2 particles from industrial high temperature processes show more spherical shapes. Fragments of the wafers can be clearly identified as artifacts by their sharp edges, glassy fracture and lack of oxygen signal.

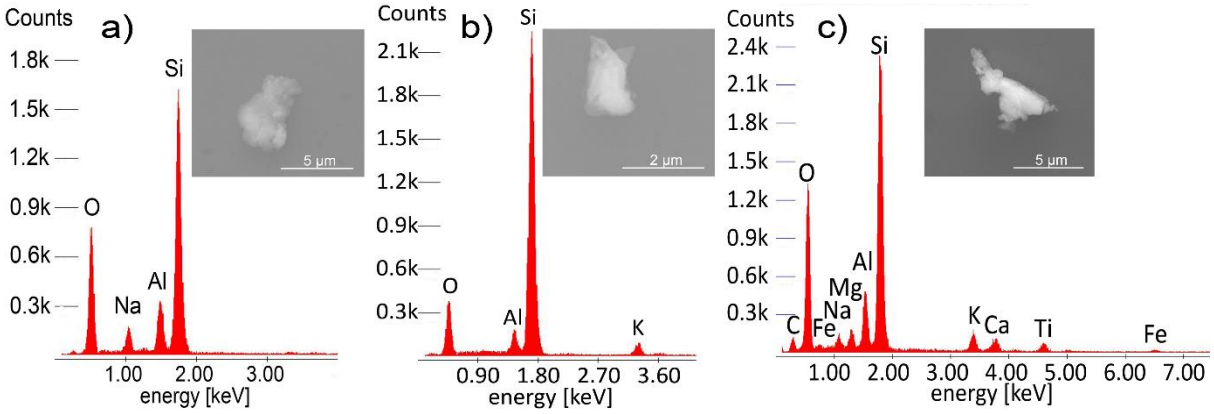

Figure 6: EDX spectra and SE-images of various aluminosilicates: a) Na-containing aluminosilicate; b) K-containing aluminosilicate; c) complex aluminosilicate

Carbonaceous particles

All particles with carbon as their main element are combined as carbonaceous particles.

The group of *biological particles*, which includes plant debris, pollen, bacteria and fungal spores as well as their fragments, can be characterized by the presence of biogenic trace elements such as P, K, Mg, Ca, Na, etc. (Ebert et al. 2000) and by their characteristic morphology. Based on our criteria, particles are only classified as biological if the bulk particle fulfills these criteria.

In many cases, *soot* particles can be clearly assigned based on their typical morphology (Fig. 7), which often shows long chains or larger agglomerates of small, spherical primary particles (Sorensen & Feke 1996). If it is not possible to characterize them by their morphology, they can be identified by their very low oxygen content compared to carbon.

The *C-rich group* contains all particles with high carbon, which cannot be clearly classified as biological particles or soot. It may also contain components from all other organic particles in the atmosphere, which can be analyzed with this method.

Other particle classes

All subgroups that cannot be clearly assigned to one of the two previous main groups are summarized as other particle classes.

The *metal oxides* are characterized by the presence of oxygen and a corresponding metal (except Al, which ich assigned to the previous aluminosilicate / Al-rich particles group). Metal oxides can originate from geogenic minerals as well as from anthropogenic sources, that is why we refrain from clearly assigning this group to mineral particles. The morphology of these particles can be either irregular (e.g., natural mineral dust, anthropogenic urban dust), or spherical, with the latter possibly originating from high-temperature processes (e.g., coal combustion) or aircraft emissions.

Sulfates are mainly characterized by the presence of sulfur and oxygen. This method can detect only beam-stable sulfates reliably. Ammonium sulfate, for example, is not beam-stable during the analysis and therefore cannot be detected reliably. The morphology of these particles varies from clean crystallization to agglomerates and irregular shapes, depending on their source and formation processes. Besides the geogenic sources (minerals like gypsum or anhydride), possible anthropogenic sources are industrial processes (mainly coal combustion), flue gas desulfurization and fertilizers. Due to the diversity of their possible sources and characteristics, we abstain from classifying them as minerals, although some of them may have a mineral origin.

All particles which are containing elements from more than one of the groups presented are assigned to *mixtures*.

Particles with gold deposits are classified as *artifacts* due to the use of gold wires as electrodes during the sampling process.

At this point, it should also be noted that our findings revealed an absence of small volatile compounds on the wafers in the EM, which are typically present in larger numbers in the total aerosol. Presumably, there is a loss of these components during sampling collection or processing. However, as these volatile particles are not known to be efficient INPs in the considered temperature range (Murray & Liu, 2022), it can be assumed that their absence does not significantly affect the results.

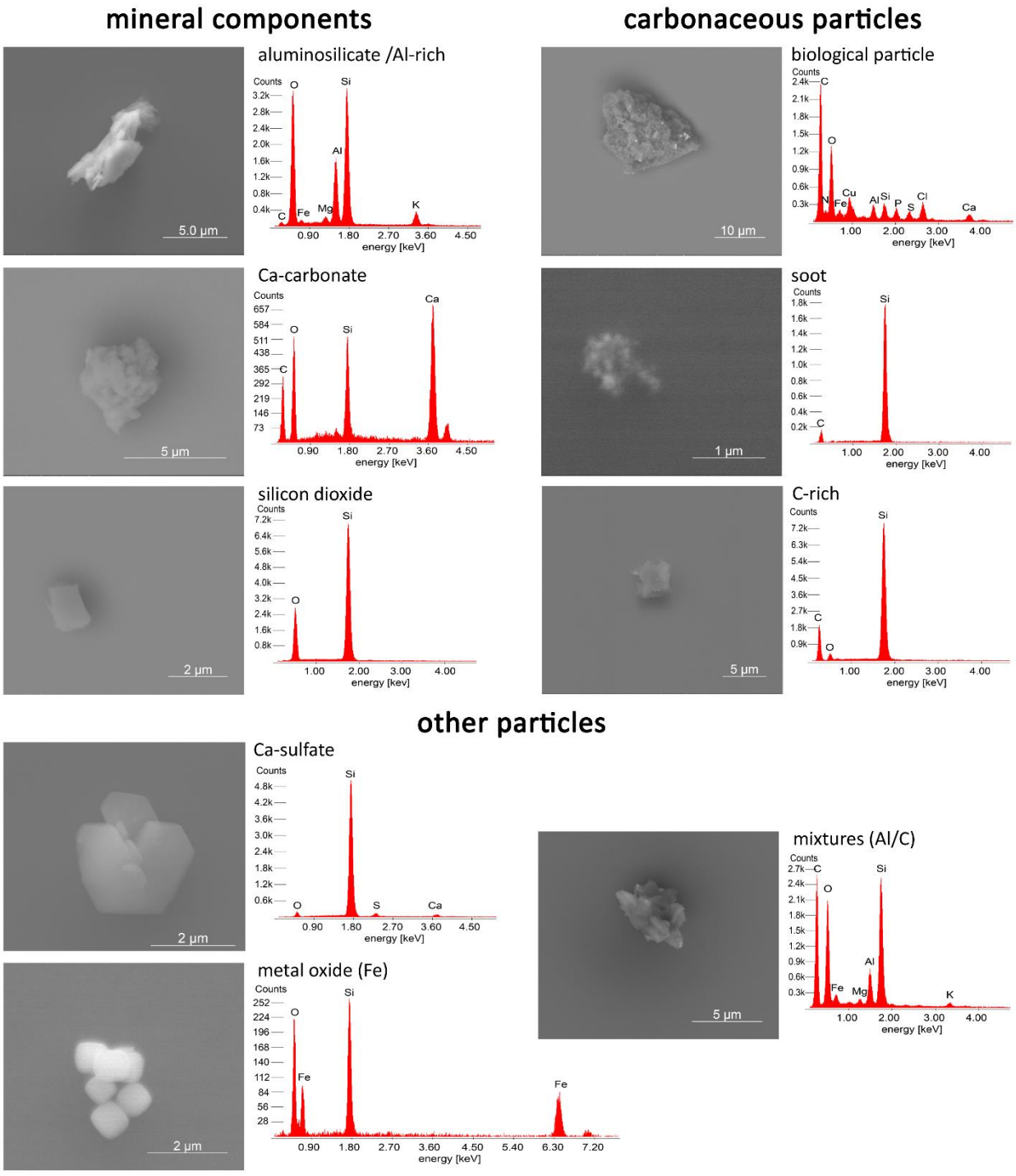

Figure 7: Overview of representative EDX spectra and corresponding images for each particle class.

3 Case Study: Results from the CLACE/INUIT campaign at the high-altitude research station Jungfraujoch in 2017

3.1 Sampling site

The high-altitude research station JFJ is located in the Swiss Alps at 3580 m above sea level between the mountain peaks of Mönch and Jungfrau. A general description of the station can be found in Bukowiecki et al. (2016). The samples were collected during the Cloud and Aerosol Characterization Experiment / Ice Nucleation Research Unit campaign (CLACE/INUIT 2017) between January 21 and February 25 2017. During winter, the station is 60 % of the time in the free troposphere (FT) (Herrmann et al., 2015), which enables characterization of the global background aerosol. A temporary influence of the planetary boundary layer is possible at any time of the year. According to Baltensperger et al. (1998) the station is in clouds (mixed-phase and ice) 40 % of the time. Since the average temperature did not fall below -15 °C during the sampling period, we assume that most INPs with activation temperatures of -20 °C to -30 °C were not activated under the prevailing environmental conditions. Even though some of them might have been activated previously in higher clouds, sampling under cloudy conditions likely does not introduce a large bias due to previously activated INPs. Aerosol sampling for the FRIDGE experiment was conducted downstream of the GAW total inlet (Lacher et al., 2021).

3.2 INP concentration & sample selection

Figure 8 illustrates the evolution of INP concentrations across the three activation temperatures, as determined by FRIDGE. The concentration for each sample is calculated on the basis of one measurement. The relative error of the counting uncertainty for individual measurements is 20 % (Schrod et al., 2016), so the error of the concentrations given here is also in this range. The concentrations observed at each temperature exhibited fluctuations of approximately one order of magnitude across the entire campaign period. Towards the end of the campaign, a Saharan dust event (SDE) was identified, which resulted in an increase in INP concentration at both -25 °C and -30 °C. This was not the case for -20 °C, as Saharan dust particles primarily activate as INPs at temperatures below -20 °C (Niemand et al., 2012, Murray et al., 2012). Since the INP concentration for -20 °C and -25 °C was sometimes very low during the campaign, we focus on the INPs activated at -30 °C for the single particle analysis. Their concentration varied between 0.1 and 1 $stdL^{-1}$ for most of the time. Based on the experience that most ice nuclei active at warmer temperatures also activate at colder temperatures, it can be assumed that only a few INPs are neglected due to limiting the analysis to INPs activated at -30 °C.

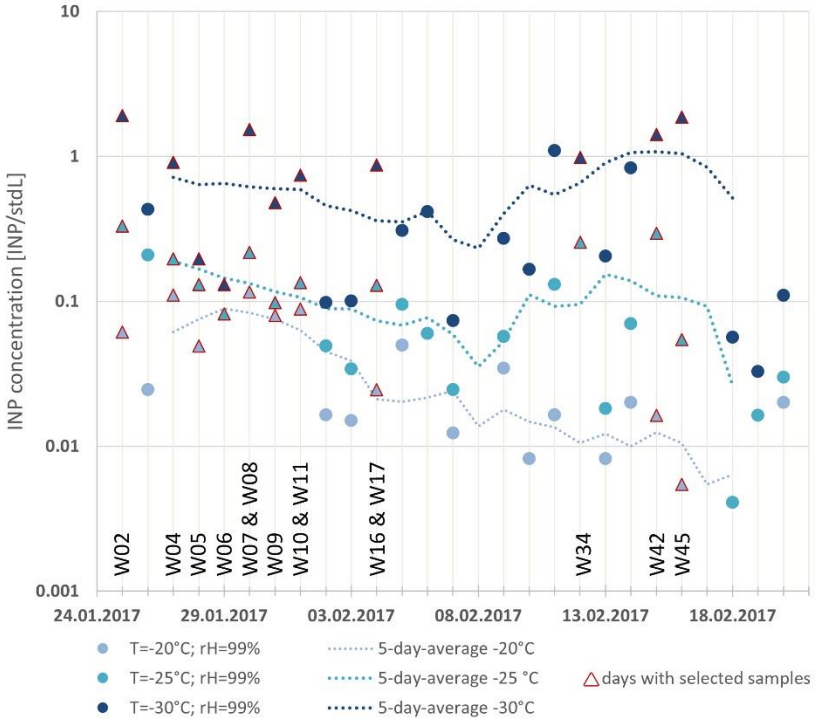

Figure 8: INP concentrations (deposition nucleation / condensation mode freezing) calculated from the FRIDGE measurements at RH = 99 % (for days with more than one sample, an average value was calculated). Days with analyzed samples are indicated by triangles and the corresponding sample numbers. The 5-day running average concentration is shown by the dotted lines (the figure is adapted from Weber (2019)).

A total of 14 substrates were selected from the larger set of samples obtained from the campaign for analysis using the coupling method presented herein. The particular samples were chosen based on their ice crystal abundance and homogeneous distribution on the substrate during the FRIDGE measurements. These samples are indicated by the corresponding sample number and triangles in Fig. 8. Overall, based on the parameters described in Sect. 2.5.2, we were able to clearly identify and characterize the associated INPs for 200 ice crystals. Although the number of identified INPs appears comparatively low for a campaign period of five weeks, these INPs were identified with a high degree of reliability (Sect. 2.5.2). The small number of particles identified bears the risk that individual, time-limited variations occurring randomly during the sampling periods may influence the resulting total composition to a certain degree. It should therefore be noted that the results presented below may not comprehensively reflect the main composition of the INPs over the entire campaign period. Nevertheless, it can be shown that the method provides valid results for the main groups of INPs (see confidence intervals for Fig. 9 in the supplement (Tab. S2)).

3.3 INP chemistry

The 200 particles identified as INP in the vicinity of the calculated coordinate were grouped into particle classes according to the classification scheme shown in Sect. 2.6. One particle with attached gold traces was classified as an artifact and therefore excluded from further discussions. The chemical composition of the remaining 199 INPs activated at -30 °C is shown in Fig. 9. Due to the limited number of identified INPs per sample (Fig. S3), mapping daily fluctuations is not possible for this campaign. Figure 9a) provides the chemical composition for all INPs sampled over the entire campaign period, within the restrictions mentioned in Sect. 3.2. Figure 9b) illustrates the methods efficacy in representing larger INP-relevant trends. Despite the small number of INPs, the SDE can be clearly recognized by a different chemical composition of the INPs from this period (confidence intervals are given in the supplement (Tab. S2)).

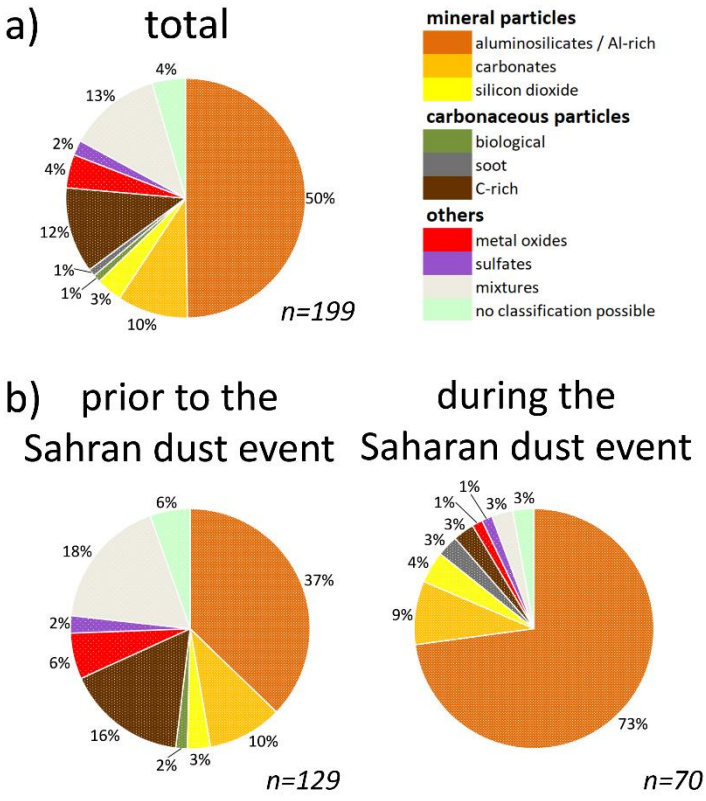

Figure 9: Chemical INP composition with the number of analyzed particles (n) from CLACE/INUIT 2017 at the high-altitude research station Jungfraujoch (activated at T = -30 °C and RH = 99 / 101 %; RH = 95 / 97 % was chosen for one sample due to cluster formation at higher RH). a) total composition over the whole campaign period; b) composition prior to and during a Saharan dust event. For confidence intervals see supplement Tab. S2.

Mineral components

The analyzed INPs sampled at the high-altitude research station JFJ in January and February 2017 were found to be predominantly composed of mineral components (63 % in total). Their proportion is 50 % prior to the SDE, rising to 86 % during the SDE. Among these, the aluminosilicate / Al-rich group increases from 37 % to 73 %, whereas the carbonates and the silicon dioxide have almost the same proportion. Throughout the entire campaign period, aluminosilicates / Al-rich particles were most prevalent, compromising 50 % of the total identified particles. These particles were present in all individual samples, except for W10, which had only one identified INP in total. Carbonates were detected in 9 individual samples (total contribution of 10 %) with Ca as the main counter ion. *Silicon dioxide* particles contributed 3 % of all identified INPs, with mostly irregular shapes indicating a geogenic origin in three samples.

These findings are in good agreement with results reported from other INP/IR measurements at the same site. Eriksen Hammer et al. (2018) and Lacher et al. (2021) observed the presence of mineral particles in comparable quantities during the same research campaign, despite analyzing IR activated between -10 °C and -18 °C. In previous campaigns Worringen et al. (2015) also identified terrigenous material as a significant contributor to ice nucleation at JFJ and Kamphus et al. (2010) observed a significant enrichment in minerals in IR compared to the total aerosol.

Carbonaceous particles

The carbon-dominated particles represented 14 % of the total INP composition during the CLACE/INUIT 2017 campaign. Only some single particles (1 % in each case) could be clearly assigned to a biological origin or soot. The remaining 12 % were classified as C-rich, and both biological material and soot, as well as any other carbonaceous particles existing in the atmosphere, may be included in this group. The fraction of carbonaceous particles decreased from 18 % before the SDE to only 6 % during the SDE.

Carbonaceous material was also identified as minor component in INPs/IRs at the high-altitude research station JFJ during winter 2013 by Worringen et al. (2015) as well as by Eriksen Hammer et al. (2018) and Lacher et al. (2021) for January and February 2017.

Other particle classes

During the CLACE / INUIT 2017 campaign metal oxides, which were primarily iron oxide, were found with a proportion of 4 % in total. A few particles within this group contained iron together with Ni and Cr as alloying elements that could be characteristic for steel. An anthropogenic origin or a local source from the station for these particles is assumed, but not confirmed. Apart from some single metal oxides with spherical shapes, most of them showed irregular shapes which may hint at a geogenic origin. Metallic particles and metal oxides have also been identified as a minor ice-forming compound by other studies conducted at the high-altitude research station JFJ (Kamphus et al., 2010; Worringen et al., 2015; Eriksen Hammer et al., 2018; Lacher et al., 2021). Ebert et al. (2011) also found metal oxides in their IRs and classified them primarily as iron oxide, which is consistent with our results.

Sulfates were rare (2 %) with Ca as the main counterion. Their morphology indicates a predominantly mineral origin.

The most abundant particle type of our mixture group features in addition to an Al peak, which is characteristic for the aluminosilicate / Al-rich group, also a distinct carbon peak (C/Al-ratio > 0.2). Most of these particles had a stronger Al-Peak with respect to the carbon peak (C/Al-ratio < 1). This Al/C-mixture may be an indication of soil dust, which contains carbonaceous material in addition to aluminosilicate / Al-rich minerals. In contrast to the aluminosilicate / Al-rich group these Al/C-mixed particles were found primarily in samples without influence of the SDE (18 % vs. 3 % during SDE), potentially pointing to a different origin of the air masses and thus a different type of mineral material (e.g., soil dust) which was transported to the station. Apart from this, the described composition can also be generated by mixing or coating with carbonaceous materials during particle aging in the atmosphere, in contrast to the freshly emitted Saharan dust. Such a mixed group at the high-altitude research station JFJ was also characterized by previous studies (Worringen et al., 2015; Ebert et al., 2011). Lacher et al. (2021) reported also that many of their mineral dust particles from the CLACE/INUIT 2017 campaign showed signals of biological material, which may be equivalent to the mixed INPs in our study.

For 4 % of all particles which can be clearly identified as INPs based on their position, no chemical classification could be performed as outlined in Sect. 2.6.

It is generally difficult to make direct comparisons between the results of different INP/IR measurement techniques, as the results can vary significantly depending on the sampling configuration, ice nucleation activation conditions, and the classification schemes used for each instrumentation. Despite these constraints and with only a limited number of identified INPs we were able to demonstrate that our method provides reliable and valid results for the main particle groups relevant to ice nucleation by comparing our main results with other INP/IR measurements performed at the high-altitude research station JFJ.

3.4 Chemically-resolved INP size distribution

In addition to providing information on the concentration and chemical composition of INPs, our coupling method offers the significant advantage of providing an INP size distribution that can be coupled to the chemistry of individual INPs. The size of each identified INP is determined by calculating the projected area diameter (d_{pa}).

Figure 10 shows the chemically-resolved size distribution of all identified INPs from the CLACE/INUIT 2017 campaign at the high-altitude research station JFJ. The graph displays the absolute INP numbers within a specific size range (blue line), with the maximum found between 1 µm and 2 µm. All particles with d_{pa} > 6 µm were summarized due to statistical purposes. In comparison to the total aerosol size distribution from the whole campaign period (Weber, 2019), the maximum of the INP size distribution is significantly shifted towards larger diameters. We hypothesize that, in addition to the primary suitability of larger particles as ice nuclei, the absence of the small volatile aerosol components (nitrates, sulfates, and volatile organics) may play a role here (see Sect. 2.6). In an enrichment and depletion study, Eriksen Hammer et al. (2018)

determined the depletion of the complex secondary aerosol in IRs compared to the total aerosol. This leads to the conclusion that the absence of these compounds does not significantly influence the results.

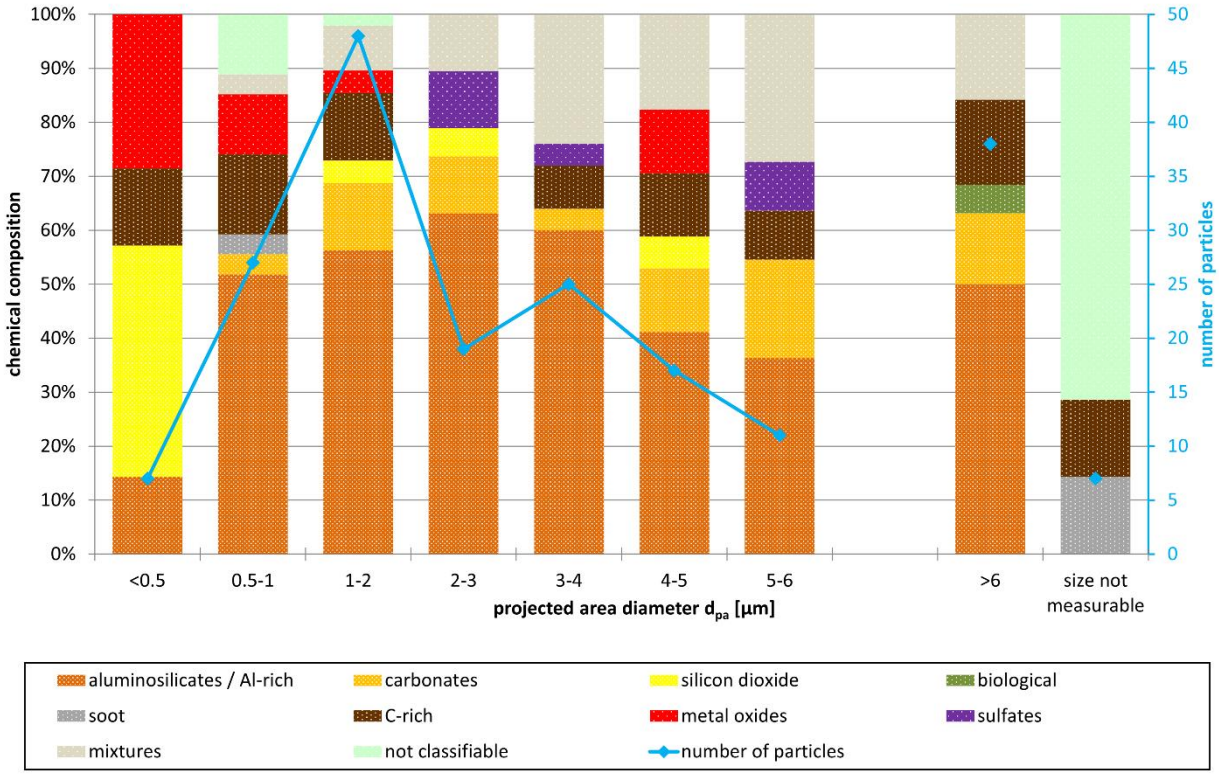

Figure 10: Chemically resolved size distribution for all identified INPs (artifact excluded; n = 199) from CLACE/INUIT 2017 at the high-altitude research station Jungfraujoch (activated at T = -30 °C and RH = 99 / 101 %; RH = 95 / 97% was chosen for one sample due to cluster formation at higher RH).

As the mineral particles (aluminosilicates / Al-rich, carbonates and silicon dioxide) are in general the most prevalent group within the analyzed samples, they are also the most prevalent group in all size ranges, with proportions ranging from 50 % to 80 %. The proportions of the individual components vary for the different size ranges. However, the aluminosilicates / Al-rich particles represent the most abundant group among all size bins from d_{pa} > 0.5 µm.

Only 3 % of the analyzed INPs had a quantifiable diameter smaller than 0.5 µm. The smallest INP whose size could be determined with confidence was 300 nm, although we can generally also see smaller particles in the SEM. This agrees to well-established findings in the literature substantiating that most particles that act as effective ice nuclei are above a size of 500 nm (DeMott et al., 2010). Besides the mineral particles, which primarily consist of silicon dioxide, the smallest size bin shows the highest proportion of metal oxides.

Significantly more particles (14 %) were found in the size range between 0.5 µm and 1 µm. In addition to the mineral fraction, carbonaceous particles as well as metal oxides and mixtures can be assigned to this size bin. However, due to their submicron size, some particles could not be chemically classified. The size range of 1-2 µm contained the largest number of INPs (24 %), with a similar chemical composition to the previous size bin.

The number of particles decreases for INPs with d_{pa} > 2 µm, which is consistent with a lower occurrence of these particles due to a reduced residence time in the free troposphere. The proportion of mixtures increases notably for INPs larger 2 µm. Additionally, C-rich particles were found in the range up to 6 µm, as well as all sulfates.

Since the abundance of INPs with d_{pa} > 6 µm is low in the individual size ranges, they are summed up. The largest INP had a d_{pa} of 34.5 µm. Apart from mineral particles, C-rich particles, and mixtures, the two biological particles were also found in this size range. Due to losses by sedimentation, long-range transport of large particles is very unlikely. However, a local influence by air that is advected from the planetary boundary layer to the station cannot be excluded.

It was not possible to determine the size of some particles, as their small size caused them to provide an insufficient image. This was the case for some carbonaceous particles, as well as for those particles for which a chemical classification was also not possible.

Lacher et al. (2021) and Worringen et al. (2015) provide size distributions for INPs/IRs measured with different techniques at the high-altitude research station JFJ up to a size of 3 µm and 5 µm, respectively. In both studies, the highest concentration was found for IRs smaller than 0.5 µm, but the broad maximum (diameters between 1.3 µm and 5 µm) from Lacher et al. (2021) agrees reasonably well to our findings. The same is the case for particles collected with the Ice Selective Inlet by Worringen et al. (2015), which also showed a secondary maximum at 1 - 1.5 µm. The shift towards larger particle diameters in our results in comparison to the maxima from Lacher et al. (2021) and Worringen et al. (2015) may be caused by the differences in sampling and ice activation. INPs in FRIDGE are activated through deposition nucleation / condensation freezing under defined conditions, while the IRs collected from ambient air are activated under natural and even more complex conditions, including the potentially more important immersion freezing mode (Ansmann et al., 2009; Murray et al., 2012).

The comparison of such INP size distributions with chemical information from different methods is difficult, since in addition to the influencing factors discussed in Sect. 3.3, a possible size selection or limitation of the sampling process, and different techniques of particle sizing may also play a role. Nevertheless, the results for our main groups are in reasonable agreement with the results from Worringen et al. (2015). In our results, both the metal oxides and the few soot particles were observed at very small diameters, which is comparable to carbonaceous particles/soot and metal oxides predominantly detected in the submicron range by Worringen et al. (2015). Terrigenous particles, including silicates and Ca-rich particles, were primarily found in the larger size ranges, while our mineral components were distributed over all size ranges, with silicates domination for particles from d_{pa} > 0.5 µm. In contrast to Worringen et al. (2015), our C-rich particles were present

over the entire size range. The reason for this is possibly that our classification scheme assigned the larger potentially biological particles as C-rich.

4 Summary and conclusions

A method for analyzing the concentration and individual physico-chemical properties of ambient INPs, which has been used in several campaigns (Schrod et al., 2020b; He et al., 2023), is discussed here from a methodological perspective. The method benefits from the coupling of two instruments already used for the analysis of INPs and IRs: the static diffusion chamber FRIDGE and the SEM. As the individual methods are already known, the focus here was on a description of the coupling and the associated advantages and uncertainties, as well as the resulting potential of the method.

Ambient atmospheric aerosol samples are collected on silicon wafer substrates using a simple electrostatic precipitator setup. Deposition nucleation and condensation freezing mode INPs are activated in the static diffusion chamber FRIDGE at various combinations of temperature and humidity and the resulting ice crystal growth is photographed. The ice crystal center points are located using an image analysis software based on the pictures taken during the FRIDGE measurement. It has been shown, that this position calculation works reasonably well, with a negligible number of incorrect positions. Engraved calibration marks are used to transfer the calculated ice crystal center point coordinates to the electron microscope. Uncertainties for the center point calculation and the calibration were discussed, with the conclusion that it is necessary to consider not only the exact coordinate but also the surrounding area. Considering the uncertainties and the desired low probability of observing multiple particles within the scan area, a scan radius of 50 µm around the calculated coordinate was established as a guideline. This limitation may lead to the exclusion of potential INPs in the case of particle drift, miscalculated ice crystal origins or more than one particle present in the scanned area. At the same time, it increases the accuracy of the results, because we are analyzing only those particles which can be unambiguously associated with the origin of a real grown ice crystal. The identification rate has been calculated to be 30 % for the presented field data, but may vary for other samples as it strongly depends on the total wafer loading. Comprehensive single particle analysis by SEM and EDX at each position where only one particle is found in the defined radius around the coordinate, provides the chemical composition of the associated INP, as well as information on its size and morphology.

Although the method has some drawbacks and uncertainties, it enables high accuracy in the identification of ice-active particles. This is, from our point of view, its significant strength compared to other INP/IR methods, which may have difficulties distinguishing between true INPs/IRs, additional collected particles, and sampling artifacts. In addition, this method can also determine ice activity for particles with a size of several micrometers, making it a useful complement to methods with size restrictions due to inlet systems or other factors. The detailed information on physico-chemical particle properties that can be obtained from SEM can be a valuable addition to pure INP counting methods for gaining information on the relevance of particle properties to ice nucleation efficiencies and could help to bridge the knowledge gap towards INP aerosol-type-specific parametrizations that could be used in modeling studies (Burrows et al., 2022).

The presented case study with samples from the CLACE/INUIT 2017 campaign at the high-altitude research station JFJ demonstrates that the method yields valuable results for the main INP classes, despite comparably low counting statistics. However, detailed statements about the minor INP classes are not possible for this study. Mineral components (aluminosilicates / Al-rich particles, carbonates and silicon dioxide), were the most prevalent as INPs in the predominantly free tropospheric air masses at the JFJ. They were distributed over the entire size range, except for silicon dioxide, which was mainly found in the size range below 500 nm. These particles originated mainly from non-local background dust sources - and in particular from a SDE, which can also be identified by a different chemical INP composition. Carbonaceous INPs of various sizes were found, including a minute amount of small soot particles as well as large biological particles. In addition, a small amount of metal oxides, mostly iron oxide, were also identified, primarily with $d_{pa} < 0.5$ µm. Sulfates were rare. Mixed particles, predominantly aluminosilicate / Al-rich particles with increased carbon content, were more common at larger diameters with a higher proportion in air masses prior to the SDE.

Future studies may relate the composition and sizes of INPs to the different activation conditions. This may help to identify which particle types and features are atmospherically most relevant as a function of temperature. The comprehensive single particle information provides also the opportunity to study for example the potential enrichment of high-effective ice nucleating particles (e.g., K-rich feldspar) by comparing the activated particles to the total wafer loading. However, due to the relatively low counting statistics, further improvements are necessary to obtain a more reliable insight into the relevance of the particle properties for the INP activation.

As experimental knowledge about concentration and composition of INPs, and their contribution to upper tropospheric ice nucleation processes in cirrus cloud formation is severely lacking (Kanji et al., 2017), the method will be adapted for future aircraft campaigns.

Data availability

The complete data set is available for the community and can be accessed by request to Martin Ebert (mebert@geo.tu-darmstadt.de) of the Technical University Darmstadt.

Author contributions

The concept of the study was designed by JC, ME and HB. The samples at the high-altitude research station Jungfraujoch were collected by DW, who also performed the FRIDGE measurements and interpreted the INP concentration data with HB, JC and JS. The scanning electron microscopy analysis was performed by LS, the interpretation was done with support from ME. KK wrote the program to perform the ice crystal center determination and coordinate conversion. The general method evaluation was done by LS, KK, HB, JS, ME. The paper concept was drafted and written by LS, with contributions from JS, DW, HB, JC, ME and KK.

Competing interests

One Co-author is member of the editorial board of the journal Atmospheric Measurement Techniques.

Acknowledgements

This work was funded by the Deutsche Forschungsgemeinschaft (DFG, German Research Foundation) – TRR 301 – Project-ID 428312742 and by the Ice nucleating research unit INUIT (FOR 1525 (project ID 170852269)).

References

Ansmann, A., Bösenberg, J., Chaikovsky, A., Comerón, A., Eckhardt, S., Eixmann, R., Freudenthaler, V., Ginoux, P., Komguem, L., Linné, H., López Marquez, M. Á., Matthias, V., Mattis, I., Mitev, V., Müller, D., Music, S., Nickovic, S., Pelon, J., Sauvage, L., Sobolewsky, P., Srivastava, M. K., Stohl, A., Torres, O., Vaughan, G., Wandinger, U., Wiegner, M.: Long-range transport of Saharan dust to norther Europe: The 11-16 October 2001 outbreak observed with EARLINET, J. Geophys. Res., 108, 4783, doi: 10.1029/1003JD003757, 2003

Ansmann, A., Tesche, M., Seifert, P., Althausen, D., Engelmann, R., Fruntke, J., Wandinger, U., Mattis, I., Müller, D.: Evolution of ice phase in tropical altocumulus: SAMUM lidar observations over Cape Verde, J. Geophys. Res., 114, D17208, doi: 10.1029/2008JD011659, 2009

Archuleta C. M., DeMott, P. J., Kreidenweis, S. M.: Ice nucleation by surrogates for atmospheric mineral dust and mineral dust/sulfate particles at cirrus temperatures, Atmos. Chem. Phys., 5, 2617-2634, doi: 10.5194/acp-5-2617-2005, 2005

Baltensperger, U., Schwikowski, M., Jost, D. T., Nyeki, S., Gäggeler, H. W., Poulida, O.: Scavenging of atmospheric constituents in mixed phase clouds at the high-alpine site Jungfraujoch Part I: Basic concept and aerosol scavenging by clouds, Atmos. Environ., Vol. 32, No. 23, 3975-3983, 1998

Boose, Y., Welti, A., Atkinson, J., Ramelli, F., Danielczok, A., Bingemer, H. G., Plötze, M., Sierau, B., Kanji, Z. A., Lohmann, U.: Heterogeneous ice nucleation on dust particles sourced from nine deserts worldwide – Part 1: Immersion freezing, Atmos. Chem. Phys., 16, 15075-15095, doi: 10.5194/acp-16-15075-2016, 2016

Brands, M., Kamphus, M., Böttger, T., Schneider, J., Drewnick, F., Roth, A., Curtius, J. Voigt, C., Borbon, A., Beekmann, M., Bourdon, A., Perrin, T., Borrmann, S.: Characterization of a Newly Developed Aircraft-Based Laser

Ablation Aerosol Mass Spectrometer (ALABAMA) and First Field Deployment in Urban Pollution Plumes over Paris During MEGAPOLI 2009, Aerosol Sci. Tech., 45:1, 46-64, doi: 10.1080/02786826.2010.517813, 2011

Brasseur, Z., Castarède, D., Thomson, E. S., Adams, M. P., Drossaart van Dusseldorp, S., Heikkilä, P., Korhonen, K., Lampilahti, J., Paramonov, M., Schneider, J., Vogel, F., Wu, Y., Abbatt, J. P. D., Atanasova, N. S., Bamford, D. H., Bertozzi, B., Boyer, M., Brus, D., Daily, M. I., Fösig, R., Gute, E., Harrison, A. D., Hietala, P., Höhler, K., Kanji, Z. A., Keskinen, J., Lacher, L., Lampimäki, M., Levula, J., Manninen, A., Nadolny, J., Peltola, M., Porter, G. C. E., Poutanen, P., Proske, U., Schorr, T., Umo, N. S., Stenszky, J., Virtanen, A., Moisseev, D., Kulmala, M., Murray, B. J., Petäjä, T., Möhler, O., Duplissy, J.: Measurement report: Introduction to the HyICE-2018 campaign for measurements of ice-nucleating particles and instrument inter-comparison in the Hyytiälä boreal forest, Atmos. Chem. Phys., 22, 5117-5145, doi: 10.5194/acp-22-5117-2022, 2022

Bukowiecki, N., Weingartner, E., Gysel, M., Collaud Coen, M, Zieger, P., Herrmann, E., Steinbacher, M., Gäggeler H. W., Baltensperger U.: A Review of More than 20 Years of Aerosol Observation at the High-Altitude Research Station Jungfraujoch, Switzerland (3580 m asl), Aerosol Air Qual. Res., 16, 764-788, doi: 10.4209/aaqr.2015.05.0305, 2016

Bundke, U., Nillius, B., Jaenicke, R., Wetter, T., Klein, H., Bingemer, H.: The fast Ice Nucleus chamber FINCH, Atmos. Res., 90, 180-186, doi: 10.1016/j.atmosres.2008.02.008, 2008

Burrows, S. M., McCluskey, C. S., Cornwell, G., Steinke, I., Zhang, K., Zhao, B., Zawadowicz, M., Raman, A., Kulkarni, G., China, S., Zelenyuk, A., DeMott, P. J.: Ice-Nucleating Particles That Impact Clouds and Climate: Observational and Modeling Research Needs, Rev. Geophys., 60, doi: 10.1029/2021RG000745, 2022

Cozic, J., Mertes, S., Verheggen, B., Cziczo, D. J., Gallavardin, S. J., Walter, S., Baltensperger, U., Weingartner, E.: Black carbon enrichment in atmospheric ice particle residuals observed in lower tropospheric mixed phase clouds, J. Geophys. Res., 113, D15209, doi: 10.1029/2007JD009266, 2008

Cziczo, D. J., Stetzer, O., Worringen, A., Ebert, M., Weinbruch, S., Kamphus, M., Gallavardin, S. J., Curtius, J., Borrmann, S. Froyd, K. D., Mertes, S., Möhler, O., Lohmann, U.: Inadvertent climate modification due to anthropogenic lead, Nat. Geosci., 2, 333-336, doi: 10.1038/ngeo499, 2009

Cziczo, D. J., Froyd, K. D., Hoose, C., Jensen, E. J., Diao, M., Zondlo, M. A., Smith, J. B., Twohy, C. H., Murphy, D. M.: Clarifying the Dominant Sources and Mechanisms of Cirrus Cloud Formation, Science, Vol. 340, 1320 – 1324, doi: 10.1126/science.1234145, 2013

Cziczo, D. J., Ladino, L., Boose, Y., Kanji, Z. A., Kupiszewski, P., Lance, S., Mertes, S., Wex, H.: Measurements of Ice Nucleating Particles and Ice Residuals, Meteor. Mon., 58, 1-13, doi: 10.1175/AMSMONOGRAPHS-D-16-0008.1, 2017

DeMott, P. J., Prenni, A. J., Liu, X., Kreidenweis, S. M., Petters, M. D., Twohy, C. H., Richardson, M. S., Eidhammer, T., Rogers, D. C.: Predicting global atmospheric ice nuclei distributions and their impacts on climate, P. Natl. A. Sci, 107, no. 25, 11217-11222, doi: 10.1073/pnas.0910818107, 2010

DeMott, P. J., Möhler, O., Cziczo, D., Hiranuma, N., Petters, M. D., Petters, S. S., Belosi, F., Bingemer, H. G., Brooks, S. D., Budke, C., Burkert-Kohn, M., Collier, K. N., Danielczok, A., Eppers, O., Felgitsch, L., Garimella, S., Grothe, H., Herenz, P., Hill, T. C. J., Höhler, K., Kanji, Z. A., Kiselev, A., Koop, T., Kristensen, T. B., Krüger, K., Kulkarni, G., Levin, E. J. T., Murray, B. J., Nicosia, A., O'Sullivan, D., Peckhaus, A., Polen, M. J., Price, H. C., Reicher, N., Rothenberg, D. A., Rudich, Y., Santachiara, G., Schiebel, T., Schrod, J., Seifreid, T. M., Stratmann, F., Sullivan, R. C., Suski, K. J., Szakáll, M., Taylor, H. P., Ullrich, R., Vergara-Temprado, J., Wagner, R., Whale, T. F., Weber, D., Welti, A., Wilson, T. W., Wolf, M. J., Zenker, J.: The Fifth International Workshop on Ice Nucleation phase 2 (FIN-02): laboratory intercomparison of ice nucleation measurements, Atmos. Meas. Tech., 11, 6231-6257, doi: 10.5194/amt-11-6231-2018, 2018

DeMott, P. J., Mirrielees, J. A., Petters, S., S., Cziczo, D. J., Petters, M. D., Bingemer, H. G., Hill, T. C. J., Froyd, K., Garimella, S., Hallar, A. G., Levin, E. J. T., McCubbin, I. B., Perring, A. E., Rapp, C. N., Schiebel, T., Schrod, J., Suski, K. J., Weber, D., Wolf, M. J., Zawadowicz, M., Zenker, J., Möhler, O., Brooks, S. D.: The Fifth International Workshop on Ice Nucleation Phase 3 (FIN-03): Field Intercomparison of Ice Nucleation Measurements, EGUsphere [preprint], doi: 10.5194/egusphere-2024-1744, 21 June 2024

Després, V. R., Huffman, J. A., Burrows, S. M., Hoose, C., Safatov A. S., Buryak G., Fröhlich-Nowoisky, J., Elbert, W., Andreae, M. O., Pöschl, U., Jaenicke, R.: Primary biological aerosol particles in the atmosphere: a review, Tellus B, 64:1, doi: 10.3402/tellusb.v64i0.15598, 2012

Ebert, M., Weinbruch, S., Hoffmann, P., Ortner, H. M.: Chemical characterization of North Sea aerosol particles, J. Aerosol Sci., Vol. 31, No. 5, 613-632, 2000

Ebert, M., Worringen, A., Benker, N., Mertes, S., Weingartner, E., Weinbruch, S.: Chemical composition and mixing-state of ice residuals sampled within mixed phase clouds, Atmos. Chem. Phys., 11, 2805-2816, doi: 10.5194/acp-11-2805-2011, 2011

Eriksen Hammer, S., Mertes, S., Schneider, J., Ebert, M., Kandler, K., Weinbruch, S.: Composition of ice particle residuals in mixed-phase clouds at Jungfraujoch (Switzerland): enrichment and depletion of particle groups relative to total aerosol, Atmos. Chem. Phys., 18, 1387-1403, doi: 10.5194/acp-18-13987-2018, 2018

Eriksen Hammer, S., Ebert, M., Weinbruch, S.: Comparison of operator- and computer-controlled scanning electron microscopy of particles from different atmospheric aerosol types, Anal. Bioanal. Chem., 411:1633-1645, doi: 10.1007/s00216-019-01614-7, 2019

He, C., Yin, Y., Huang, Y., Kuang, X., Cui, Y., Chen, K., Jiang, H., Kiselev, A., Möhler, O., Schrod, J.: The Vertical Distribution of Ice-Nucleating Particles over the North China Plain: A Case of Cold Front Passage, Remote Sens., 15, 4989, doi: 10.3390/rs15204989, 2023

Herrmann, E., Weingartner, E., Henne, S., Vuilleumier, L., Bukowiecki, N., Steinbacher, M., Conen, F., Collaud Coen, M., Hammer, E., Jurányi, Z., Baltensperger, U., Gysel, M.: Analysis of long-term aerosol size distribution data from Jungfraujoch with emphasis on free tropospheric conditions, cloud influence, and air mass transport, J. Geophys. Res.-Atmos., 9459 – 9480, doi: 10.1002/201JD023660, 2015

Hiranuma, N., Augustin-Bauditz, S., Bingemer, H., Budke, C., Curtius, J., Danielczok, A., Diehl, K., Dreischmeier, K., Ebert, M., Frank, F., Hoffmann, N., Kandler, K., Kiselev, A., Koop, T., Leisner, T., Möhler, O., Nillius, B., Peckhaus, A., Rose, D., Weinbruch, S., Wex, H., Boose, Y., DeMott, P. J., Hader, J. D., Hill, T. C. J., Kanji, Z. A., Kulkarni, G., Levin, E. J. T., McCluskey, C. S., Murakami, M., Murray, B. J., Niedermeier, D., Petters, M. D., O'Sullivan D., Saito, A., Schill, G. P., Tajiri, T., Tolbert, M. A., Welti, A., Whale, T. F., Wright T. P., Yamashita, K.: A comprehensive laboratory study on the immersion freezing behavior of illite NX particles: a comparison of 17 ice nucleation measurement techniques, Atmos. Chem. Phys., 15, 2489-2518, doi: 10.5194/acp-15-2489-2015, 2015

Hiranuma, N., Adachi, K., Bell, D. M., Belosi, F., Beydoun, H., Bhaduri, B., Bingemer, H., Budke, C., Clemen, H.-C., Conen, F., Cory, K. M., Curtius, J., DeMott, P. J., Eppers, O., Grawe, S., Hartmann, S., Hoffmann, N., Höhler, K., Jantsch, E., Kiselev, A., Koop, T., Kulkarni, G., Mayer, A., Murakami, M., Murray, B. J., Nicosia, A., Petters, M. D., Piazza, M., Polen, M., Reicher, N., Rudich, Y., Saito, A., Santachiara, G., Schiebel, T., SChill, G. P., Schneider, J., Segev, L., Stopelli, E:, Sullivan, R. C., Suski, K., Szakáll, M., Tajiri, Z., Taylor, H., Tobo, Y., Ullrich, R., Weber, D., Wex, H., Whale, T. F., Whiteside, C. L., Yamashita, K., Zelenyuk, A., Möhler, O.: A comprehensive characterization of ice nucleation by three different types of cellulose particles immersed in water, Atmos. Chem. Phys., 19, 4823-4849, doi: 10.5194/acp-19-4823-2019, 2019

Hoose, C. and Möhler, O.: Heterogeneous ice nucleation on atmospheric aerosols: a review of results from laboratory experiments, Atmos. Chem. Phys., 12, 9817-9854, doi: 10.5194/acp-12-9817-2012, 2012

Jing, X., Yang, J., Li, T., Hu, J., He, C., Yin, Y., DeMott, P. J., Wang, Z., Jiang, H., Chen, K.: Pre-Activation of Ice Nucleating Particles in Deposition Nucleation Mode: Evidence from Measurement Using a Static Vacuum Water Vapor Diffusion Chamber in Xinjiang, China, Geophys. Res. Lett., 49, e2022GL099468, doi: 10.1029/2022GL099468, 2022

Kamphus, M., Ettner-Mahl, M., Klimach, T., Drewnick, F., Keller, L., Cziczo, D. J., Mertes, S., Borrmann, S., Curtius, J.: Chemical composition of ambient aerosol, ice residues and cloud droplet residues in mixed-phase clouds: single particle analysis during the Cloud and Aerosol Characterization Experiment (CLACE 6), Atmos. Chem. Phys., 10, 8077-8095, doi: 10.5194/acp-10-8077-2010, 2010

Kandler, K., Benker, N., Bundke, U., Cuevas, E., Ebert, M., Knippertz, P., Rodríguez, E., Schütz, L., Weinbruch, S.: Chemical composition and complex refractive index of Saharan Mineral Dust at Izaña, Tenerife (Spain) derived by electron microscopy, Atmos. Environ. 41, 8058-8074, doi: 10.1016/j.atmosenv.2007.06.047, 2007

Kanji, Z. A., Florea, O., Abbatt, J. P. D.: Ice formation via deposition nucleation on mineral dust and organics: dependence of onset relative humidity on total particulate surface area, Environ. Res. Lett., 3, 025004, doi: 10.1088/1748-9326/3/2/025004, 2008

Kanji, Z. A., Ladino, L. A., Wex, H., Boose, Y., Burkert-Kohn, M., Cziczo, D. J., Krämer, M.: Overview of Ice Nucleating Particles, Meteor. Mon., Vol. 58, doi: 10.1175/AMSMONOGRAPHS-D-16-0006.1, 2017

Kiselev, A., Bachmann, F., Pedevilla, P., Cox, S. J., Michaelides, A., Gerthsen, D., Leisner, T.: Active sites in heterogeneous ice nucleation – the example of K-rich feldspars, Science, 10, doi: 10.1126/science.aai8034, 2016

Klein, H., Haunold, W., Bundke, U., Nillius, B., Wetter, T., Schallenberg, S., Bingemer, H.: A new method for sampling of atmospheric ice nuclei with subsequent analysis in a static diffusion chamber, Atmos. Res., 96, 218-224, doi: 10.1016/j.atmores.2009.08.002, 2010

Kupiszewski, P., Weingartner, E., Vochezer, P., Schnaiter, M., Bigi, A., Gysel, M., Rosati, B., Toprak, E., Mertes, S., Baltensperger, U.: The Ice Selective Inlet. A novel technique for exclusive extraction of pristine ice crystals in mixed-phase clouds, Atmos. Meas. Tech., 8, 3087-3106, doi: 10.5194/amt-8-3087-2015, 2015

Kupiszewski, P., Zanatta, M., Mertes, S., Vochezer, P., Lloyd, G., Schneider, J., Schenk, L., Schnaiter, M., Baltensperger, U., Weingartner, E., Gysel, M.: Ice residual properties in mixed-phase clouds at the high-alpine Jungfraujoch site, J. Geophys. Res.-Atmos, 121, 12343-12362, doi: 10.1002/2016JD024894, 2016

Lacher, L., Clemen H.-C., Shen, X., Mertes, S., Gysel-Beer, M., Moallemi, A., Steinbacher, M., Henne, S., Saathoff, H., Möhler, O., Höhler, K., Schiebel, T., Weber, D., Schrod, J., Schneider, J., Kanji, Z. A.: Sources and nature of ice-nucleating particles in the free troposphere at Jungfraujoch in winter 2017, Atmos. Chem. Phys., 21, 16925-16953, doi: 10.5194/acp-21-16925-2021, 2021

Lacher, L., Adams, M. P., Barry, K., Bertozzi, B., Bingemer, H., Boffo, C., Bras, Y., Büttner, N., Castarede, D., Cziczo, D. J., DeMott, P. J., Fösig, R., Goodell, M., Höhler, K., Hill, T. C. J., Jentzsch, C., Ladino, L. A., Levin, E. J. T., Mertes, S., Möhler, O., Moore, K. A., Murray, B. J., Nadolny, J., Pfeuffer, T., Picard, D., Ramírez-Romero, C., Ribeiro, M., Richter, S., Schrod, J., Sellegri, K., Stratmann, F., Swanson, B. E., Thomson E. S., Wex, H., Wolf, M. J., Freney, E.: The Puy de Dôme ICe Nucleation Intercomparison Campaign (PICNIC): comparison between online and offline methods in ambient air, Atmos. Chem. Phys., 24, 2651-2678, doi: 10.5194/ACP-24-2651-2024, 2024

Marcolli, C.; Pre-activation of aerosol particles by ice preserved in pores, Atmos. Chem. Phys., 17, 1595-1622, doi: 10.5194/acp-17-1595-2017, 2017

Mertes, S., Verheggen, B., Walter, S., Connolly, P., Ebert, M., Schneider, J., Bower, K. N., Cozic, J., Weinbruch, S., Baltensperger, U., Weingartner, E.: Counterflow Virtual Impactor Based Collection of Small Ice Particles in Mixed-Phase Clouds for the Physico-Chemical Characterization of Tropospheric Ice Nuclei: Sampler Description and First Case Study, Aerosol Sci. Tech., 41, 848-864, doi: 10.1080/02786820701501881, 2007

Murray, B. J., O'Sullivan, D., Atkinson, J. D., Webb, M. E.: Ice nucleation by particles immersed in supercooled cloud droplets, Chem. Soc. Rev., 41, 6519-6554, doi: 10.1039/c2cs35200a, 2012

Murray, B. J. and Liu, X.: Ice-nucleating particles and their effects on clouds and radiation, in: Aerosols and Climate, edited by Carslaw, K. S., Elsevier, 619-649, doi:10.1016/B978-0-12-819766-0.00014-6, 2022

Niemand, M., Möhler, O., Vogel, B., Vogel, H., Hoose, C., Connolly, P., Klein, H., Bingemer, H., DeMott, P., Skrotzki, J., Leisner, T.: A Particle-Surface-Area-Based Parametrization of Immersion Freezing on Desert Dust Particles, J. Atmos. Sci, 69 (10), 3077-3092, doi: 10.1175/JAS-D-11_0249.1, 2012

Okada, K. and Kai, K.: Atmospheric mineral particles collected at Qira in the Taklamakan Desert, China, Atmos. Environ. 38, 6927-6935, doi: 10.1016/j.atmosenv.2004.03.078, 2004

O'Sullivan, D., Murray, B. J., Malkin, T. L., Whale, T. F., Umo, N. S., Atkinson, J. D., Price, H. C., Baustian, K. J., Browse, J., Webb, M. E.: Ice nucleation by fertile soil dusts: relative importance of mineral and biogenic components, Atmos. Chem. Phys., 14, 1853-1867, doi: 10.5194/acp-14-1853-2014, 2014

Perry, K. D., Cahill, T. A., Eldred, R. A., Dutcher, D. D.: Long-range transport of North African dust to the eastern United States, J. Geophys. Res., 102, 11,225-11,238, doi: 10.1029/97JD00260, 1997

Pratt, K. A., DeMott, P. J., French, J. R., Wang, Z., Westphal, D. L., Heymsfield, A. J., Twohy, C. H., Prenni, A. J., Prather, K. A.: In situ detection of biological particles in cloud ice-crystals, Nat. Geosci., Vol. 2, 398 – 401, doi: 10.1038/NGEO521, 2009

Prenni, A. J., Petters, M. D., Kreidenweis, S. M., Heald, C. L., Martin, S. T., Artaxo, P., Garland, R. M., Wolly, A. G., Pöschl, U.: Relative roles of biogenic emissions and Saharan dust and ice nuclei in the Amazon basin, Nat. Geosci., Vol. 2, 402-405, doi: 10.1038/NGEO517, 2009

Pummer, B. G., Bauer, H., Bernardi, J., Bleicher, S., Grothe, H.: Suspendable macromolecules are responsible for ice nucleation activity of birch and conifer pollen, Atmos. Chem. Phys., 12, 2541-2550, doi: 10.5194/acp-12-2541-2012, 2012

Rogers, D. C.: Development of a Continuous Flow Thermal Gradient Diffusion Chamber for Ice Nucleation Studies, Atmos. Res., 22, 149-181, 1988

Schenk, L. P., Mertes, S., Kästner, U., Frank, F., Nillius, B., Bundke, U., Rose, D., Schmidt, S., Schneider, J., Worringen, A., Kandler, K., Bukowiecki, N., Ebert, M., Curtius, J., Stratmann, F.: Characterization and first results of an ice nucleating particle measurement system based on counterflow virtual impactor technique, Atmos. Meas. Tech. Discuss., 7, 10585-10617, doi: 10.5194/amtd-7-10585-2014, 2014

Schepanski, K.: Transport of Mineral Dust and Its Impact on Climate, Geosiences 2018, 8, 151, doi: 10.3390/geoscience8050151, 2018

Scheuvens, D. and Kandler, K.: On Composition, Morphology, and Size Distribution of Airborne Mineral Dust, in: Mineral Dust, edited by Knippertz, P. and Stuut, J.-B. W., Springer, Dordrecht, doi: 10.1007/978-94-017-8978-3_2, 2014

Schmidt, S., Schneider, J., Klimach, T., Mertes, S., Schenk, L. P., Kupiszewski, P., Curtius, J., Borrmann, S.: Online single particle analysis of ice particle residuals from mountain-top mixed-phase clouds using laboratory derived particle type assignment, Atmos. Chem. Phys., 17, 575-594, doi: 10.5194/acp-17-575-2017, 2017

Schneider, C. A., Rasband, W. S., Eliceiri, K. W., NIH Image to ImageJ: 25 years of image analysis, Nat. Methods, 9(7), 671-675, doi: 10.1038/nmeth.2089, 2012

Schrod, J., Danielczok, A., Weber, D., Ebert, M., Thomson E. S., Bingemer H. G.: Re-evaluating the Frankfurt isothermal static diffusion chamber for ice nucleation, Atmos. Meas. Tech., 9, 1313-1324, doi: 10.5194/amt-9-1313-2016, 2016

Schrod, J., Weber, D., Drücke, J., Keleshis, C., Pikridas, M., Ebert, M., Cvetkovic, B., Nickovic, S., Marinou, E., Baars, H., Ansmann, A., Vrekoussis, M., Mihalopoulos, N., Sciare, J., Curtius, J., Bingemer, H. G.: Ice nucleating particles over the Eastern Mediterranean measured by unmanned aircraft systems, Atmos. Chem. Phys., 17, 4817-4835, doi: 10.5194/acp-17-4817-2017, 2017

Schrod, J., Kleinhenz, D., Hörhold, M., Erhardt, T., Richter, S., Wilhelms F., Fischer, H., Ebert, M., Twarloh, B., Della Lunga, D., Jensen, C. M., Curtius, J., Bingemer, H. G.: Ice-nucleating particle concentrations of the past: insights from a 600-year-old Greenland ice core, Atmos. Chem. Phys., 20, 12459-12482, doi: 10.2194/acp-20-12459-2020, 2020a

Schrod, J., Thomson E. S., Weber, D., Kossmann, J., Pöhlker, C., Saturno J., Ditas, F., Artaxo, P., Clouard, V., Saurel, J.-M., Ebert, M., Curtius, J., Bingemer, H. G.: Long-term deposition and condensation ice-nucleating particle measurements from four stations across the globe, Atmos. Chem. Phys., 20, 15983 – 16006, doi: 10.5194/acp-20-15983-2020, 2020b

Schwarzenboeck, A., Heintzenberg, J., Mertes, S.: Incorporation of aerosol particles between 25 and 850 nm into cloud elements: measurments with a new complementary sampling system, Atmos. Res., 25, 241-260, doi: 10.1016/S0169-8059(99)00034-4, 2000

Sorensen, C. M., Feke, G. D.: The Morphology of Macroscopic Soot, Aerosol Sci. Tech., 25, 328-337, doi:10.1080/02786829608965399, 1996

Thomson, D. S., Schein, M. E., Murphy, D. M.: Particle Analysis by Laser Mass Spectrometry WB-57F Instrument Overview, Aerosol Sci. Tech., 33:153-169, doi: 10.1080/027868200410903, 2000

Vali, G., DeMott, P. J., Möhler, O., Whale, T. F.: Technical Note: A proposal for ice nucleation terminology, Atmos. Chem. Phys., 15, 10263 – 10270, doi: 10.5194/acp-15-10263-2015, 2015

Wilson, T. W., Ladino, L. A., Alpert, P. A., Breckels, M. N., Brooks, I. M., Browse, J., Burrows, S. M., Carslaw, K. S., Huffman, J. A., Judd, C., Kilthau, W. P., Mason, R. H., McFiggans, G., Miller, L. A., Nájera J. J., Polishchuk, E., Rae, S., Schiller, C. L., Si, M., Vergara Temprado, J., Whale, T. F., Wong, J. P. S., Wurl, O., Yakobi-Hancock, J. D., Abbatt, J. P. D., Aller, J. Y., Bertram, A. K., Knopf, D. A., Murray, B. J.: A marine biogenic source of atmospheric ice-nucleating particles, Nature 525, 234-238, doi: 10.1038/nature14986, 2015

Weber, D.: Eisnukleation von Aerosolen: Laborexperimente und Messungen im Feld, Ph.D. thesis, Goethe Universität Frankfurt, Germany, 2019

Welti, A., Lüönd, F., Stetzer, O., Lohmann, U.: Influence of particle size on the ice nucleating ability of mineral dusts, Atmos. Chem. Phys., 9, 6705-6715, doi: 10.5194/acp-9-6705-2009, 2009

Wex, H., Huang, L., Zhang, W., Hung, H., Traversi, R., Becagli, S., Sheesley, R. J., Moffett, C. E., Barrett, T. E., Bossi, R., Skov, H., Hünerbein, A., Lubitz, J., Löffler, M., Linke, O., Hartmann, M., Herenz, P., Stratmann, F.: Annual variability of ice-nucleating particle concentrations at different Arctic locations, Atmos. Chem. Phys., 19, 5293-5311, doi: 10.5194/acp-19-5293-2019, 2019

Whalley, W. B. and Krinsley, D. H.: A scanning electron microscope study of surface textures of quartz grains from glacial environments, Sedimentology, 21, 87-105, doi:10.1111/j.1365-3091.1974.tb01783.x, 1974

Worringen, A., Kandler, K., Benker, N., Dirsch, T., Mertes, S., Schenk, L., Kästner, U., Frank, F., Nillius, B., Bundke, U., Rose, D., Curtius, J., Kupiszewski, P., Weingartner, E., Vochezer, P., Schneider, J., Schmidt, S. Weinbruch, S., Ebert, M.: Single-particle characterization of ice-nucleating particles and ice particle residuals sampled by three different techniques, Atmos. Chem. Phys., 15, 4161-4178, doi: 10.5194/acp-15-4161-2015, 2015

940 Yakobi-Hancock, J. D., Ladino, L. A., Abbatt, J. P. D.: Feldspar minerals as efficient deposition ice nuclei, Atmos.Chem. Phys., 13, 11175-11185, doi: 10.5194/acp-13-11175-2013, 2013